

Exercise reduces inflammatory cell production and cardiovascular inflammation via instruction of hematopoietic progenitor cells

Vanessa Frodermann^{1,14}, David Rohde^{1,14}, Gabriel Courties¹, Nicolas Severe^{2,3}, Maximilian J. Schloss¹, Hajera Amatullah⁴, Cameron S. McAlpine¹, Sebastian Cremer¹, Friedrich F. Hoyer¹, Fei Ji^{5,6}, Ian D. van Koeverden⁷, Fanny Herisson¹, Lisa Honold¹, Gustavo Santos Masson¹, Shuang Zhang¹, Jana Grune¹, Yoshiko Iwamoto¹, Stephen P. Schmidt¹, Gregory R. Wojtkiewicz¹, I-Hsiu Lee¹, Karin Gustafsson^{2,3}, Gerard Pasterkamp⁸, Saskia C. A. de Jager^{1,7,9}, Ruslan I. Sadreyev^{6,10}, Jean MacFadyen¹¹, Peter Libby¹¹, Paul Ridker¹¹, David T. Scadden^{2,3}, Kamila Naxerova¹, Kate L. Jeffrey⁴, Filip K. Swirski¹ and Matthias Nahrendorf^{1,12,13*}

A sedentary lifestyle, chronic inflammation and leukocytosis increase atherosclerosis; however, it remains unclear whether regular physical activity influences leukocyte production. Here we show that voluntary running decreases hematopoietic activity in mice. Exercise protects mice and humans with atherosclerosis from chronic leukocytosis but does not compromise emergency hematopoiesis in mice. Mechanistically, exercise diminishes leptin production in adipose tissue, augmenting quiescence-promoting hematopoietic niche factors in leptin-receptor-positive stromal bone marrow cells. Induced deletion of the leptin receptor in *Prrx1*-creER^{T2}, *Lepr*^{f/f} mice reveals that leptin's effect on bone marrow niche cells regulates hematopoietic stem and progenitor cell (HSPC) proliferation and leukocyte production, as well as cardiovascular inflammation and outcomes. Whereas running wheel withdrawal quickly reverses leptin levels, the impact of exercise on leukocyte production and on the HSPC epigenome and transcriptome persists for several weeks. Together, these data show that physical activity alters HSPCs via modulation of their niche, reducing hematopoietic output of inflammatory leukocytes.

Even though cardiovascular therapeutics have advanced rapidly, the number of patients globally with atherosclerosis and its complications is on the rise. Changes in lifestyle including an unhealthy diet, low physical activity and obesity, contribute to this worldwide epidemic. Despite current management strategies, many individuals still develop first or recurrent cardiovascular events, such as myocardial infarction (MI), stroke, heart failure or limb ischemia. Mechanistically, inflammation accounts for some of this residual risk¹. Indeed, the Canakinumab Anti-inflammatory Thrombosis Outcomes Study (CANTOS) documented that targeting inflammatory pathways, specifically the cytokine interleukin-1 β , can lower cardiovascular events in selected patients already receiving aggressive management, including highly effective statin treatment².

The cellular protagonists of arterial wall inflammation include leukocytes of several classes, notably macrophages, monocytes and neutrophils. Monocyte and neutrophil blood counts associate with cardiovascular disease (CVD) progression and death³. Because these cells only live for a day or less, their production rates influence systemic cell abundance and recruitment to cardiovascular organs.

Hence, understanding the signals that lead to overproduction of inflammatory leukocytes may provide strategies to reduce inflammatory cardiovascular events⁴.

Leukocytes derive from HSPCs. HSPCs may increase proliferation and thus leukocyte production in response to cytokines, growth factors and danger signals. Recent research has unraveled mechanisms that influence hematopoiesis in CVD by illuminating pathways through which hyperlipidemia⁵, psychosocial stress⁶, insufficient sleep⁷ and obesity⁸ increase HSPC proliferation and the bone marrow's myeloid cell output. These well-known risk factors act either directly on HSPCs or via the hematopoietic niche, an ensemble of stromal bone marrow cells that protects HSPCs and instructs their proliferation, migration and lineage bias⁹.

Sedentary lifestyle is a risk factor for MI, whereas physical activity seems to protect against CVD¹⁰. One observational study followed 55,137 adults over 15 years and reported that persistent running was associated with 50% lower cardiovascular mortality¹¹. Most available data¹⁰ indicate that this relationship rests on metabolic and antihypertensive effects that counter the aging

¹Center for Systems Biology, Department of Radiology, Massachusetts General Hospital, Harvard Medical School, Boston, MA, USA. ²Department of Stem Cell and Regenerative Biology, Harvard University, Cambridge, MA, USA. ³Center for Regenerative Medicine and Cancer Center, Massachusetts General Hospital, Boston, MA, USA. ⁴Gastrointestinal Unit and Center for the Study of Inflammatory Bowel Disease, Massachusetts General Hospital, Harvard Medical School, Boston, MA, USA. ⁵Department of Genetics, Harvard Medical School, Boston, MA, USA. ⁶Department of Molecular Biology, Massachusetts General Hospital, Boston, MA, USA. ⁷Laboratory of Experimental Cardiology, Department of Cardiology, University Medical Center Utrecht, Utrecht, the Netherlands. ⁸Laboratory for Clinical Chemistry and Haematology, University Medical Center Utrecht, Utrecht, the Netherlands. ⁹Laboratory of Translational Immunology, University Medical Center Utrecht, Utrecht, the Netherlands. ¹⁰Department of Pathology, Massachusetts General Hospital, Harvard Medical School, Boston, MA, USA. ¹¹Division of Cardiovascular Medicine, Department of Medicine, Brigham and Women's Hospital and Harvard Medical School, Boston, MA, USA. ¹²Cardiovascular Research Center, Massachusetts General Hospital, Harvard Medical School, Boston, MA, USA. ¹³Department of Internal Medicine I, University Hospital Wuerzburg, Wuerzburg, Germany. ¹⁴These authors contributed equally: Vanessa Frodermann, David Rohde. *e-mail: mnahrendorf@mgh.harvard.edu

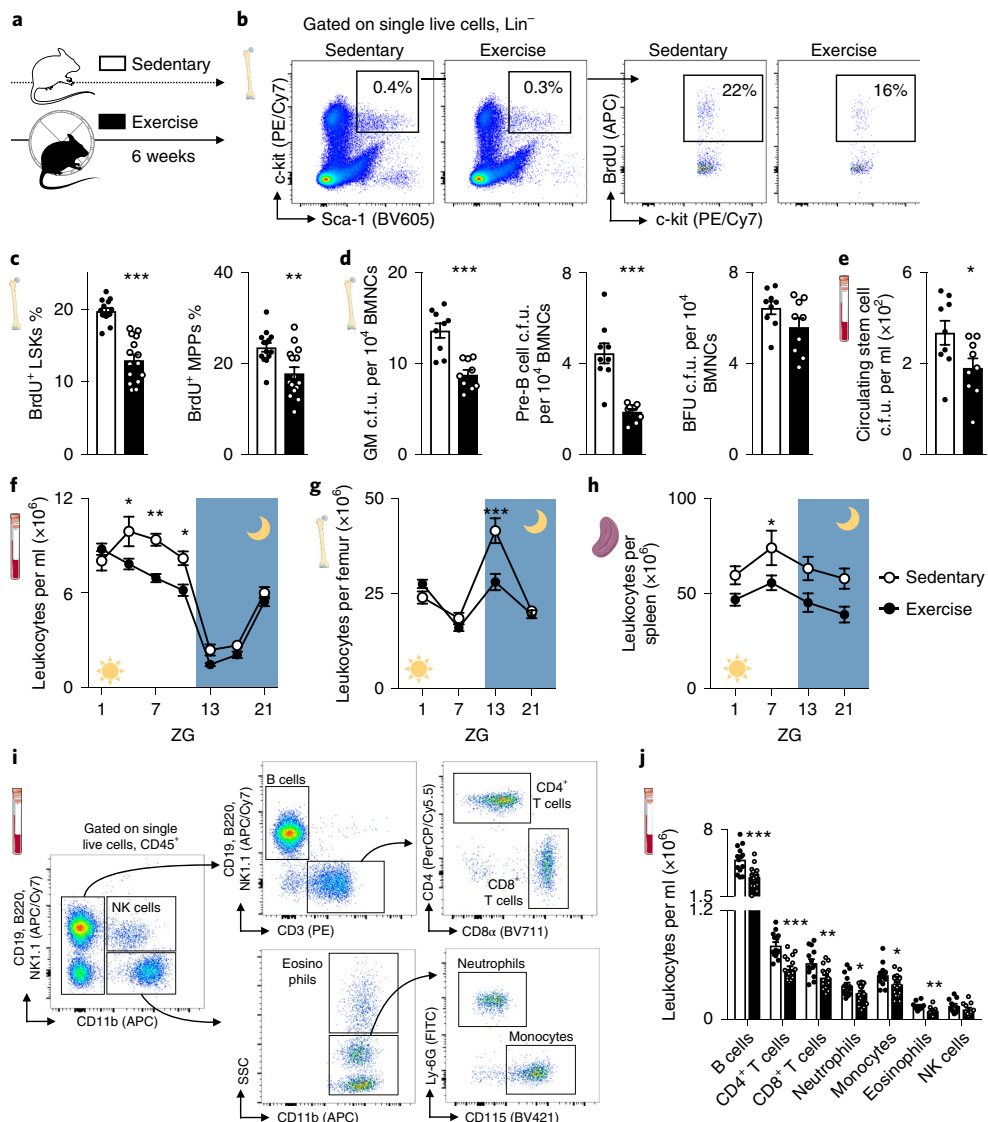
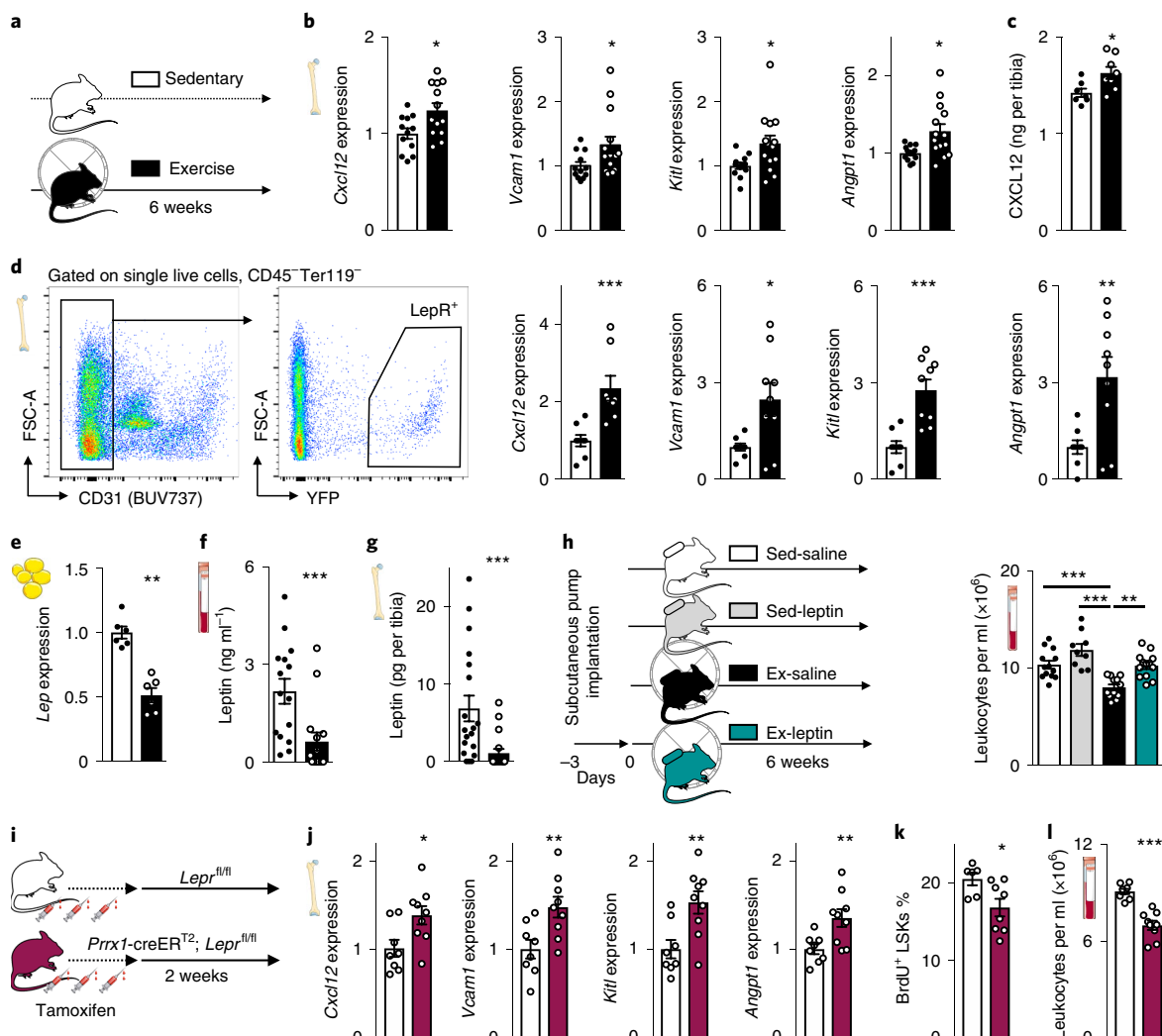


Fig. 1 | Exercise increases HSPC quiescence. **a**, Experimental outline. Hematopoietic parameters were measured in C57BL/6 mice that had access to exercise wheels for 6 weeks (exercise) or not (sedentary). **b,c**, Proliferation of hematopoietic stem and progenitor cells (LSKs) and MPPs, as analyzed by BrdU incorporation using flow cytometry. Representative dot plots for LSK (**b**) and statistical analysis (**c**) are shown ($^{**}P=0.0023$, $^{***}P=4.25 \times 10^{-8}$; $n=14$ sedentary and $n=15$ exercising animals; four independent experiments; two-tailed Student's *t*-test). **d**, A c.f.u. assay of bone marrow mononuclear cells (BMNCs) for granulocytes and macrophages (GMs), pre-B cells and burst-forming unit-erythroid cells (BFUs) ($^{***}P=0.00012$ for GMs, $^{***}P=4.22 \times 10^{-5}$ for preB cells, $P=0.052$ for BFUs; $n=9$ animals per group; data were analyzed by two-tailed Student's *t*-test). **e**, Circulating stem cells measured by c.f.u. assay for complete colonies ($^{*}P=0.018$; $n=9$ animals per group; two independent experiments were performed; data were analyzed by two-tailed Student's *t*-test). **f**–**h**, Circadian rhythm of leukocyte numbers in the blood (**f**) ($^{*}P=0.029$ for zeitgeber time (ZG) 5, $^{*}P=0.038$ for ZG 9, $^{**}P=0.0025$ for ZG 7; $n=12$ animals for ZG 1, 5, 7, and 21, $n=8$ animals for ZG 13 and 17, for sedentary, $n=17$ animals for ZG 1, $n=18$ animals for ZG 5, 7, 9 and 21, $n=12$ animals for ZG 13 and 17, for exercise; three independent experiments were conducted; data were analyzed by two-way analysis of variance (ANOVA) with Sidak's post hoc test); bone marrow (**g**) ($^{***}P=2.14 \times 10^{-6}$; $n=8$ and $n=11$ animals for ZG 1, $n=8$ and $n=12$ animals for ZG 7, for sedentary and exercise, respectively, $n=9$ animals per group for ZG 13, $n=3$ animals per group for ZG 21; eight independent experiments were conducted; data were analyzed by two-way ANOVA with Sidak's post hoc test); and spleen (**h**) ($^{*}P=0.012$; $n=4$ and $n=5$ animals for ZG 1, $n=7$ animals and $n=12$ animals for ZG 7, for sedentary and exercise, respectively, $n=6$ animals per group for ZG 13, $n=3$ animals per group for ZG 21; four independent experiments were conducted; data were analyzed by two-way ANOVA with Sidak's post hoc test). **i**, Flow cytometry gating for blood leukocytes at ZG 7. **j**, Leukocyte subsets in circulation at ZG 7 ($^{*}P=0.044$ for neutrophils, $^{*}P=0.019$ for monocytes, $^{**}P=0.0025$ for CD8⁺ T cells, $^{**}P=0.0057$ for eosinophils, $^{***}P=0.00022$ for B cells, $^{***}P=4.96 \times 10^{-6}$ for CD4⁺ T cells; $n=14$ and $n=18$ animals for B cells, T cells and monocytes, $n=14$ and $n=17$ animals for neutrophils, $n=10$ and $n=12$ animals for eosinophils and natural killer (NK) cells, for sedentary and exercise, respectively; four independent experiments were conducted; data were analyzed by two-tailed Student's *t*-test, comparing sedentary and exercise for each cell subset). Data are mean \pm s.e.m. We acknowledge Servier Medical Art (<https://smart.servier.com>) for providing images of mice and cartoon components.

processes; however, the mechanisms by which physical activity could mitigate cardiovascular inflammation remain uncertain. Exercise has clear effects on the immune¹² and cardiovascular^{13–15} systems. Whether and how regular physical activity

affects the hematopoietic system is incompletely understood. We therefore studied the hematopoietic system, which is well characterized in mice, as a function of regular voluntary physical activity.



Results

Voluntary running promotes HSPC quiescence. To explore whether regular physical activity modulates hematopoiesis and

the systemic supply of leukocytes, we provided mice with running wheels, which they used avidly (Extended Data Fig. 1a,b), for 6 weeks (Fig. 1a). Habitual voluntary running, which increases

activity 20-fold compared to sedentary mice¹⁶, reduced body weight, augmented food consumption (Extended Data Fig. 1c–e) and did not change skeletal muscle leukocyte recruitment (Extended Data Fig. 1f,g) or bone architecture (Extended Data Fig. 1h–k). Voluntary running promoted HSPC quiescence: Lin⁻Sca-1⁺c-kit⁺ cells (LSKs) proliferated 34% less, as assessed by 5-bromo-2- deoxyuridine (BrdU) incorporation (Fig. 1b,c). The reduction in proliferation occurred at the stage of multipotent progenitors (MPPs), a subset of LSKs (Fig. 1c) and in all leukocyte progenitors, regardless of myeloid or lymphoid lineage (Extended Data Fig. 2a–d). BrdU washout assays confirmed that all progenitors downstream of CD48⁻CD150⁺ long-term hematopoietic stem cells (LT-HSCs) and CD48⁻CD150⁻ short-term HSCs (ST-HSCs) proliferated less in running mice (Extended Data Fig. 2e,f). Progenitors formed fewer myeloid and lymphoid colonies, whereas the erythroid lineage was less affected (Fig. 1d and Extended Data Fig. 2g,h). Running mice mobilized fewer HSPCs to the circulation from the bone marrow (Fig. 1e), which, when viewed together with decreased differentiation into mature leukocytes (Extended Data Fig. 2i), explains why HSPC numbers in the bone marrow were preserved (Extended Data Fig. 2j).

The hematopoietic effects of exercise reduced circulating leukocyte numbers (Fig. 1f–j). Differences between running and sedentary cohorts peaked at zeitgeber time (ZG) 7 in the blood (Fig. 1f), indicating decreased leukocyte release when mice rest, and at ZG 13 in the bone marrow (Fig. 1g), indicating reduced nocturnal leukocyte production. Physical activity lowered all leukocyte subsets (Fig. 1i,j and Extended Data Fig. 2i). We further observed a decrease in platelets but not in red blood cells, hemoglobin or hematocrit (Extended Data Fig. 2k). We found that voluntary running did not change the bone marrow's autonomic nervous system activity, as mass spectrometry documented unchanged bone marrow norepinephrine and acetylcholine concentration (Extended Data Fig. 3a). We similarly did not observe any differences in local leukocyte acetylcholine production (Extended Data Fig. 3b) after

muscarinic cholinergic receptor inhibition (Extended Data Fig. 3c) or in levels of the stress hormone corticosterone (Extended Data Fig. 3d). Given the habitual voluntary running wheel use by mice in our study, higher blood leukocyte levels in sedentary mice indicate that lack of physical activity in humans partially confers cardiovascular risk via increased systemic leukocyte supply.

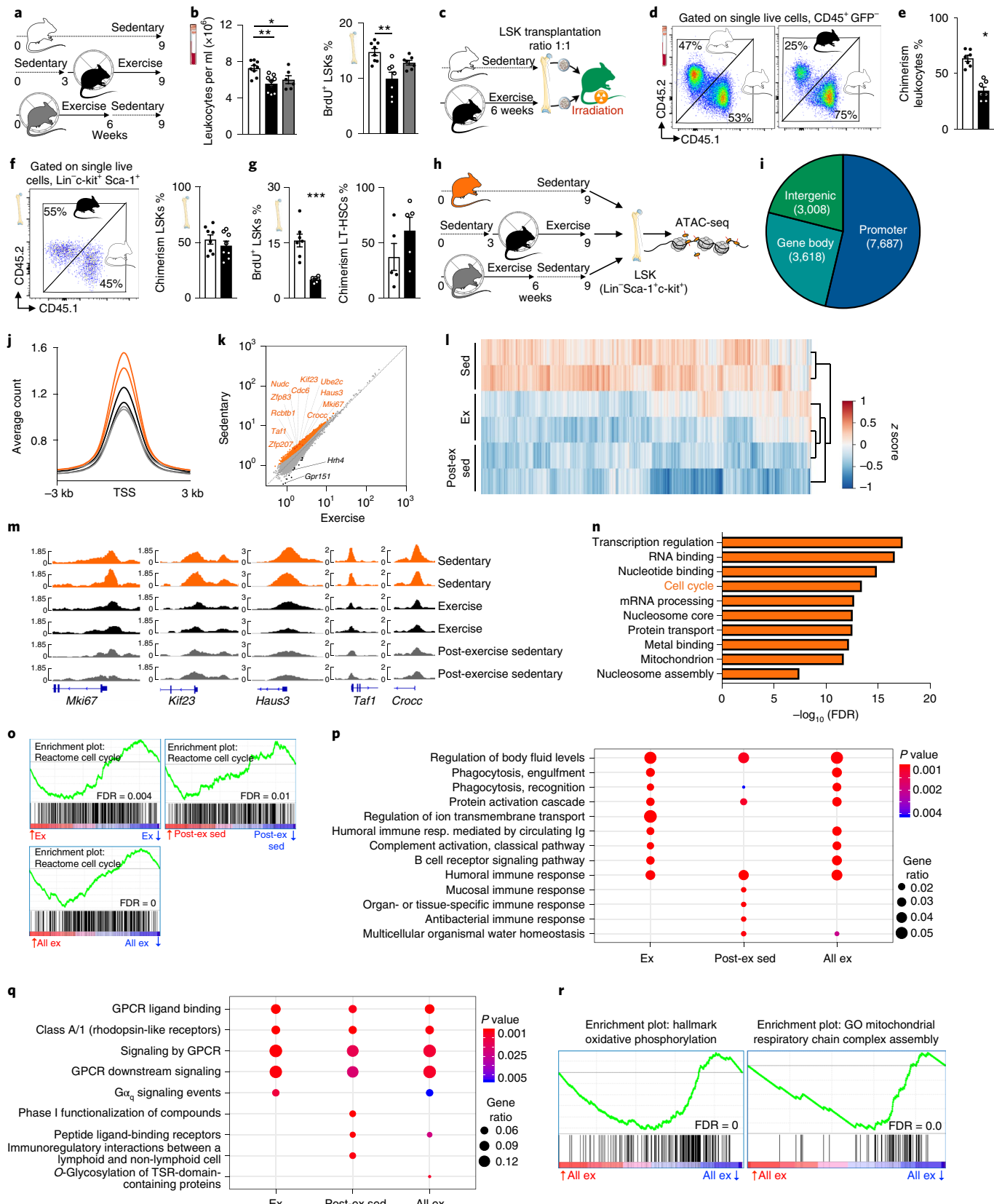
Exercise increases CXCL12 in the hematopoietic niche via lowering leptin. To investigate how physical activity alters leukocyte supply, we examined the hematopoietic niche that instructs HSPC activity^{9,17}. The bone marrow of exercising mice displayed increased expression of important HSPC quiescence and retention genes, specifically *Cxcl12*, *Vcam1*, *Kitl* and *Angpt1*, as well as increased CXCL12 protein levels (Fig. 2a–c). It is well understood that these signals instruct hematopoiesis in many settings^{9,17}; however, their modulation by physical activity was previously unknown. We next assessed gene expression among key stromal cells defining the hematopoietic niche. In running mice, only leptin receptor (LepR⁺) stromal cells (assessed using *Lepr*-YFP mice) expressed more *Cxcl12*, *Vcam1*, *Kitl* and *Angpt1* (Fig. 2d). Expression of these genes did not change in other hematopoietic niche cells, including nestin⁺ mesenchymal cells (*Nes*-GFP mice), osteocalcin (OCN)⁺ osteoblastic cells (*Bglap*-GFP mice), endothelial cells and macrophages (Extended Data Fig. 3e–h). Overall niche cell numbers did not differ between sedentary and exercising mice (Extended Data Fig. 3i). Expression of other niche factors (*Csf1*, *Csf2*, *Csf3*, *Ccl2*, *Il7*, *Tgfb1* and *Pf4*) and adipocyte-specific (*Lpl* and *Fabp4*) and osteolineage-specific (*Sp7*, *Bglap* and *Runx2*) genes was unaltered (Extended Data Fig. 3j,k).

Hematopoietic niche profiling indicated that LepR⁺ stromal cells relay exercise effects; hence, we investigated potential pathways related to the hormone leptin, which decreases appetite and is a proinflammatory adipokine¹⁸. Exercise reduced body fat (Extended Data Fig. 4a) and adipose tissue expression of inflammatory cytokines (Extended Data Fig. 4b), as well as adipose

Fig. 3 | Voluntary running reduces LSK chromatin accessibility. **a**, Experimental outline for **b**. Sedentary control C57BL/6 J mice had no access to exercise wheels (top); the exercise group had access to wheels during the last 6 weeks before sacrifice (middle); and the post-exercise sedentary group had access to wheels for 6 weeks, after which the wheels were removed for the following 3 weeks (bottom). **b**, Circulating leukocyte levels (left) (* $P=0.033$, ** $P=0.0025$; $n=9$ animals for sedentary and exercise, $n=6$ animals for post-exercise sedentary; three independent experiments were conducted; data were analyzed by Kruskal-Wallis test with Dunn's post hoc test) at ZG 7 and BrdU incorporation in LSKs, as measured 22 h after intraperitoneal injection (right) (** $P=0.0043$; $n=8$ animals for sedentary, $n=7$ animals for exercise and post-exercise sedentary; two independent experiments were conducted; data were analyzed by Kruskal-Wallis test with Dunn's post hoc test). **c**, Experimental outline of the competitive bone marrow transplantation experiments in **d–g**. LSKs were isolated from donors that either had exercised for 6 weeks (CD45.2) or were sedentary (CD45.1^{STEM}) and were then transplanted in a 1:1 ratio into irradiated *ubiquitin C* (*Ubc*)-GFP recipients. **d**, Flow cytometry plots of circulating leukocytes after transplantation. Plots are shown for a control that received LSKs from a sedentary CD45.2 mouse and a sedentary CD45.1^{STEM} mouse (left) and the experimental group as shown in **c** (right). **e**, Blood chimerism 4 weeks after transplantation (* $P=0.016$; $n=7$ animals per group; data were analyzed by Wilcoxon matched-pairs signed-rank test). **f**, Dot plot and quantification of bone marrow LSK chimerism ($n=8$ animals per group). **g**, BrdU incorporation in LSKs 22 h after intraperitoneal injection (left) (** $P=0.0006$; $n=7$ animals per group; two independent experiments were conducted; data were analyzed by two-tailed Mann-Whitney U-test); and LT-HSC chimerism (right) ($n=5$ animals per group). Data are mean \pm s.e.m. **h**, Experimental outline for **i–n**. LSKs were isolated from the experimental groups in **a** and subjected to ATAC-seq analysis. **i**, Genomic distribution of ATAC-seq peaks (numbers in pie chart) in LSKs among genes, promoters, enhancers and other intergenic regions. **j**, Profiles of average ATAC-seq tag density over all TSS-proximal regions (TSS \pm 3 kb) in LSKs. Each curve refers to an individual mouse; see **h** for color coding. **k**, Scatterplot of normalized tag density at ATAC-seq peaks comparing LSKs from sedentary versus exercise cohorts. Peaks with significantly lower and higher tag density in running mice are highlighted in orange and black, respectively (FDR < 0.01). The top ten key genes in the cell cycle pathway, as determined by DAVID (refer to **n**) and *Mki67* are indicated; see Supplementary Table 1 for all genes. **l**, Patterns of chromatin accessibility among 3,605 TSS-proximal peaks (TSS \pm 3 kb) with differential ATAC-seq signal between conditions (FDR < 0.01). Heat map color indicates the ATAC-seq tag density relative to the average across all samples for the given peak. **m**, Tracks of normalized ATAC-seq tag density for the *Mki67*, *Kif23*, *Haus3*, *Taf1* and *Crocc* loci. **n**, Functional pathway categories of differential chromatin accessibility in sedentary versus exercising mice as determined by DAVID. **o**, Enrichment analysis of the gene set 'Reactome cell cycle' in RNA-seq data of LSKs from mice in exercise and post-exercise sedentary versus sedentary groups. Genes were ranked by \log_2 (fold change). **p,q**, GO biological process categories (**p**) and Reactome gene sets (**q**) enriched in genes that were at least twofold downregulated in exercising mice versus sedentary mice. The gene ratio is the fraction of tested genes belonging to each gene set. P values are from the hypergeometric distribution. resp., response; GPCR, G-protein-coupled receptor; TSR, thrombospondin type 1 repeat. **r**, Enrichment analysis of gene sets related to oxidative phosphorylation in LSKs from exercising versus sedentary mice. Genes were ranked by \log_2 (fold change). Experimental groups in **o–r** are as shown in **a**. All FDR values were calculated with the Benjamini-Hochberg procedure. We acknowledge Servier Medical Art (<https://smart.servier.com>) for providing images of mice and cartoon components.

tissue macrophage numbers and their proliferation (Extended Data Fig. 4c–e). In running mice, visceral adipose tissue produced less leptin (Fig. 2e), leading to decreased levels of the hormone in blood and bone marrow (Fig. 2f,g). While exercise led to smaller bone

marrow adipocytes in the red bone marrow of the proximal tibia, adipocyte differentiation and numbers did not change (Extended Data Fig. 4f–h) and the overall bone marrow fat content remained constant (Extended Data Fig. 4i,j). Leptin expression in the bone



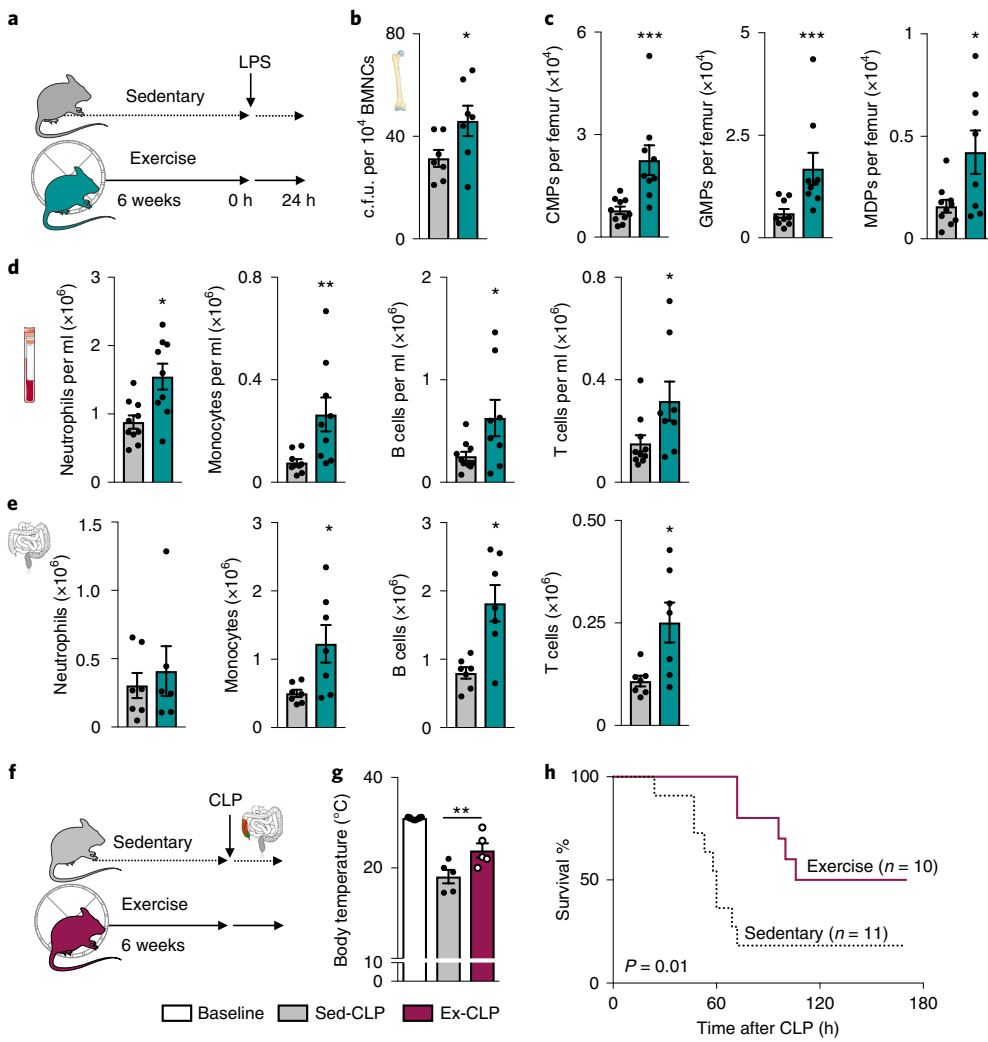


Fig. 4 | Exercise augments emergency hematopoiesis and improves survival in sepsis. **a**, Experimental outline for **b–e**. C57BL/6J mice received intraperitoneal injections of LPS after 6 weeks of exercise or no exercise. Analysis was performed 24 h after LPS injection. **b**, Bone marrow c.f.u. assay of BMNCs (* $P=0.048$; $n=7$ animals per group; two independent experiments were conducted; data were analyzed by two-tailed Mann–Whitney *U*-test). **c**, Bone marrow common myeloid progenitors (CMPs), GMPs and macrophage dendritic cell progenitors (MDPs) 24 h after LPS injection (* $P=0.018$, *** $P=0.0004$ for CMPs, *** $P=0.0008$ for GMPs; $n=10$ animals for sedentary, $n=9$ animals for exercise; three independent experiments were conducted; data were analyzed by two-tailed Mann–Whitney *U*-test). **d**, Numbers of neutrophils (* $P=0.01$), monocytes (** $P=0.0028$), B cells (* $P=0.038$) and T cells (* $P=0.04$) in the circulation ($n=10$ and $n=9$ animals for neutrophils and monocytes, $n=10$ and $n=8$ animals for B cells and T cells, for sedentary and exercise, respectively; three independent experiments were conducted; data were analyzed by two-tailed Mann–Whitney *U*-test). **e**, Number of leukocytes in the peritoneal cavity after injection of LPS (* $P=0.038$ for monocytes, * $P=0.011$ for B cells, * $P=0.018$ for T cells; $n=7$ and $n=6$ animals for neutrophils, for sedentary and exercise, respectively, $n=7$ per group for monocytes, B cells and T cells; two independent experiments were conducted; data were analyzed by two-tailed Mann–Whitney *U*-test). **f**, Experimental outline for **g** and **h**. Cecal ligation and puncture (CLP) was induced after 6 weeks of exercise or in sedentary controls. **g**, Body core temperature was measured before CLP surgery (baseline) and 48 h after CLP (** $P=0.0043$; $n=6$ animals for baseline and $n=5$ animals for each CLP group; two independent experiments were conducted; data were analyzed by two-tailed Mann–Whitney *U*-test comparing sedentary and exercise groups post-CLP). Data are mean \pm s.e.m. **h**, Survival after CLP (* $P=0.012$; $n=11$ sedentary and $n=10$ exercise mice post-CLP; three independent experiments were conducted; data were analyzed by Mantel–Cox log-rank test). We acknowledge Servier Medical Art (<https://smart.servier.com>) for providing images of mice and cartoon components.

marrow was low and unaffected by exercise (Extended Data Fig. 4k) and the leptin concentration in bone marrow did not correlate with the size of tibial adipocytes (Extended Data Fig. 4l), supporting a prominent role of visceral fat as the source of leptin.

Viewing these data together with previous reports that leptin deficiency impairs hematopoiesis¹⁹, that leptin levels correlate with leukocytes in adolescent Japanese males²⁰ and that exercise reduces leptin levels²¹, we reasoned that exercise-induced changes in hematopoiesis may result from reduced adipose-tissue-derived leptin. To test this hypothesis, we elevated leptin levels to those seen

in sedentary mice during exercise using minipump supplementation (Fig. 2h and Extended Data Fig. 5a). This intervention restored circulating leukocytes (Fig. 2h) and LSK proliferation (Extended Data Fig. 5b), whereas bone marrow *Cxcl12*, *Vcam1* and *Angpt1* expression declined to the levels seen in sedentary mice (Extended Data Fig. 5c). The chosen leptin concentration did not affect the running distance (Extended Data Fig. 5d). In sedentary mice, leptin-neutralizing antibody treatment reduced hematopoiesis, whereas leptin injections had the opposite effect (Extended Data Fig. 5e).

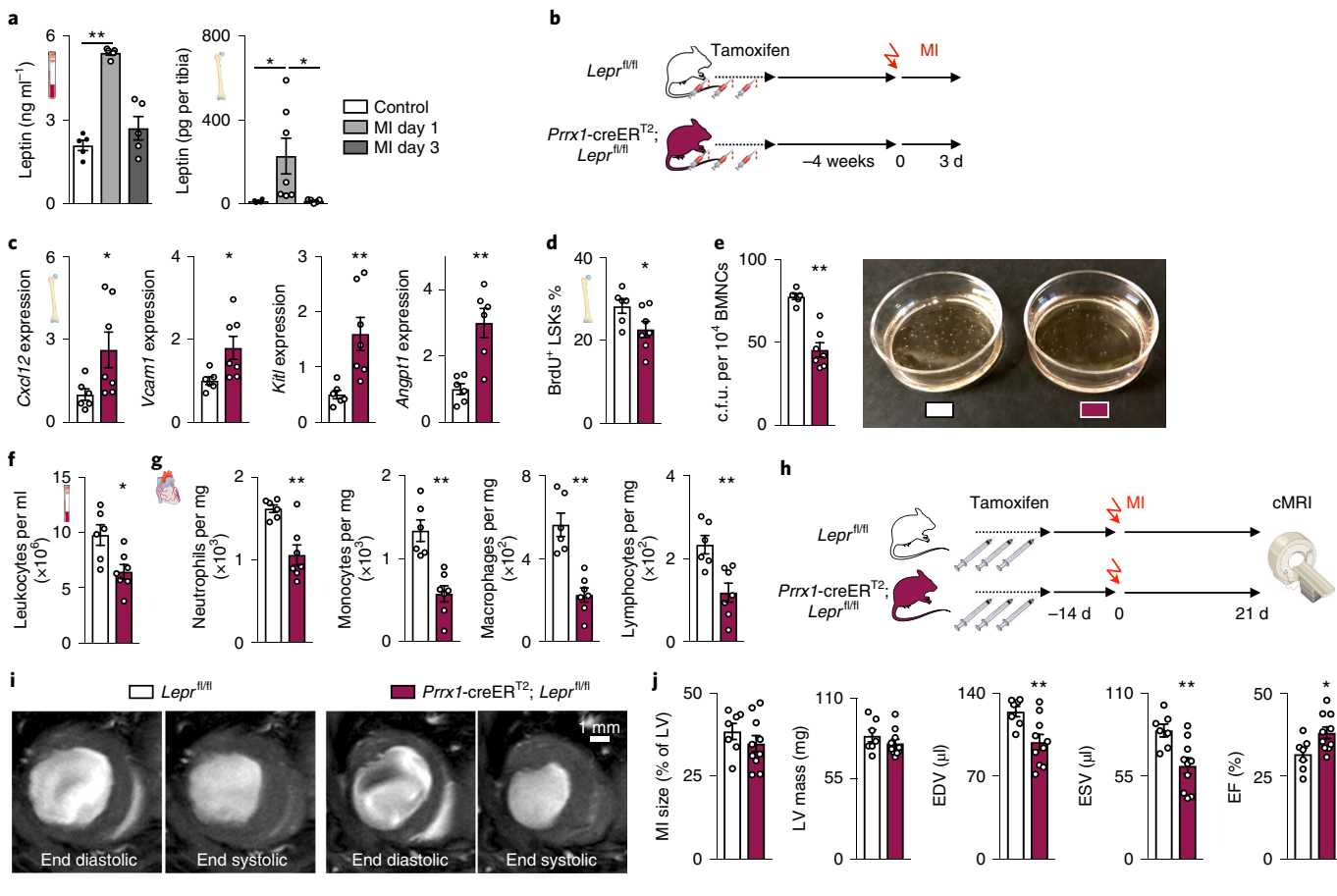


Fig. 5 | Disrupting leptin signaling reduces hematopoiesis and inflammation in acute MI. **a**, Serum leptin levels (left) (**P=0.0089; n=5 animals per group; Kruskal-Wallis test with Dunn's post hoc test) and bone marrow leptin levels (right) (*P=0.017 for control versus MI day 1, *P=0.015 for MI day 1 versus MI day 3; n=4 animals for control, n=7 animals for MI day 1, n=5 animals for MI day 3; data were analyzed by Kruskal-Wallis test with Dunn's post hoc test) at day 1 or 3 after MI in C57BL/6J mice or naive controls, as measured by ELISA. **b**, Experimental outline for **c–g**. *Prrx1-creER^{T2}, Lep^{f/f}* mice or their *Lepr^{f/f}* littermates had MI 4 weeks after being injected three times with tamoxifen every other day. Mice were killed 3 d after MI. **c**, Gene expression in total bone marrow, as measured by PCR (*P=0.035 for *Cxcl12*, *P=0.014 for *Vcam1*, **P=0.0023 for *Kitl*, **P=0.0087 for *Angpt1*; n=6 animals for *Lepr^{f/f}* and n=7 animals for *Prrx1-creER^{T2}, Lep^{f/f}*; two independent experiments were conducted; data were analyzed by two-tailed Mann-Whitney U-test). mRNA levels were normalized to *Actb* Ct values. **d**, BrdU incorporation into LSKs 22 h after intraperitoneal injection, as measured by flow cytometry (*P=0.022; n=6 animals for *Lepr^{f/f}* and n=7 animals for *Prrx1-creER^{T2}, Lep^{f/f}*; two independent experiments were conducted; data were analyzed by two-tailed Mann-Whitney U-test). **e**, Bone marrow c.f.u. assay of BMNCs for complete colonies (left) (**P=0.0012; n=6 animals for *Lepr^{f/f}* and n=7 animals for *Prrx1-creER^{T2}, Lep^{f/f}*; two independent experiments were conducted; data were analyzed by two-tailed Mann-Whitney U-test) and a representative image of the assay (right). **f**, Circulating leukocyte levels (*P=0.022; n=6 animals for *Lepr^{f/f}* and n=7 animals for *Prrx1-creER^{T2}, Lep^{f/f}*; two independent experiments were conducted; data were analyzed by two-tailed Mann-Whitney U-test). **g**, Neutrophil (**P=0.0082), monocyte (**P=0.0012), macrophage (**P=0.0012) and lymphocyte (**P=0.0047) numbers in the infarct (n=6 animals for *Lepr^{f/f}* and n=7 for *Prrx1-creER^{T2}, Lep^{f/f}*; two independent experiments were conducted; data were analyzed by two-tailed Mann-Whitney U-test). **h**, Experimental outline for **i–j**. Mice received three tamoxifen injections every other day and had an MI 2 weeks later. Cardiac magnetic resonance imaging (cMRI) was performed 3 weeks after MI. **i,j**, Cardiac MRI in *Prrx1-creER^{T2}, Lep^{f/f}* mice and their *Lepr^{f/f}* littermates: representative short-axis images (**i**) and statistical analysis (**j**) (**P=0.0097 for end diastolic volume (EDV), **P=0.0046 for end systolic volume (ESV), *P=0.043 for ejection fraction (EF); n=7 animals for *Lepr^{f/f}* and n=10 animals for *Prrx1-creER^{T2}, Lep^{f/f}*; three independent experiments were conducted; data were analyzed by two-tailed Mann-Whitney U-test). LV, left ventricle. We acknowledge Servier Medical Art (<https://smart.servier.com>) for providing images of mice and cartoon components.

Previous reports state that short-term ablation of LepR⁺ stromal cells and deletion of niche factors in LepR⁺ cells deplete HSCs^{22,23}. However, constitutive LepR deficiency in stromal cells does not affect hematopoiesis but rather remodels the bone marrow niche²⁴. Leptin may also act directly on HSPCs¹⁹. Therefore, we aimed to clarify how leptin affects hematopoiesis: via direct action on HSPCs or indirectly via LepR⁺ stromal cells in the hematopoietic niche. Using *Lepr*-tdTomato reporter mice, we profiled hematopoietic and stromal bone marrow cells by flow cytometry. While there was a distinct tdTomato⁺ stromal cell population expressing LepR, leukocytes and HSPCs were negative for tdTomato (Extended Data Fig. 6a–c). Adding increasing concentrations of leptin to a colony-forming unit (c.f.u.) assay did not change

the number of colonies (Extended Data Fig. 6d). Further, the effects of exercise on hematopoiesis were preserved in wild-type mice that had received lethal irradiation followed by bone marrow transplantation from *db/db* mice that lack LepR (Extended Data Fig. 6e–i). Tamoxifen-induced, stromal-cell-specific deletion of LepR in adult *Prrx1-creER^{T2}, Lep^{f/f}* mice, which show no differences in systemic leptin levels (Extended Data Fig. 6j), increased expression of HSPC maintenance niche factors in the bone marrow, reduced LSK proliferation and decreased circulating leukocytes (Fig. 2i–l), corresponding to an exact phenocopy of running mice. Developmental compensation likely accounts for the differences between our observations 2 weeks after tamoxifen-induced LepR deletion in adult mice and previously

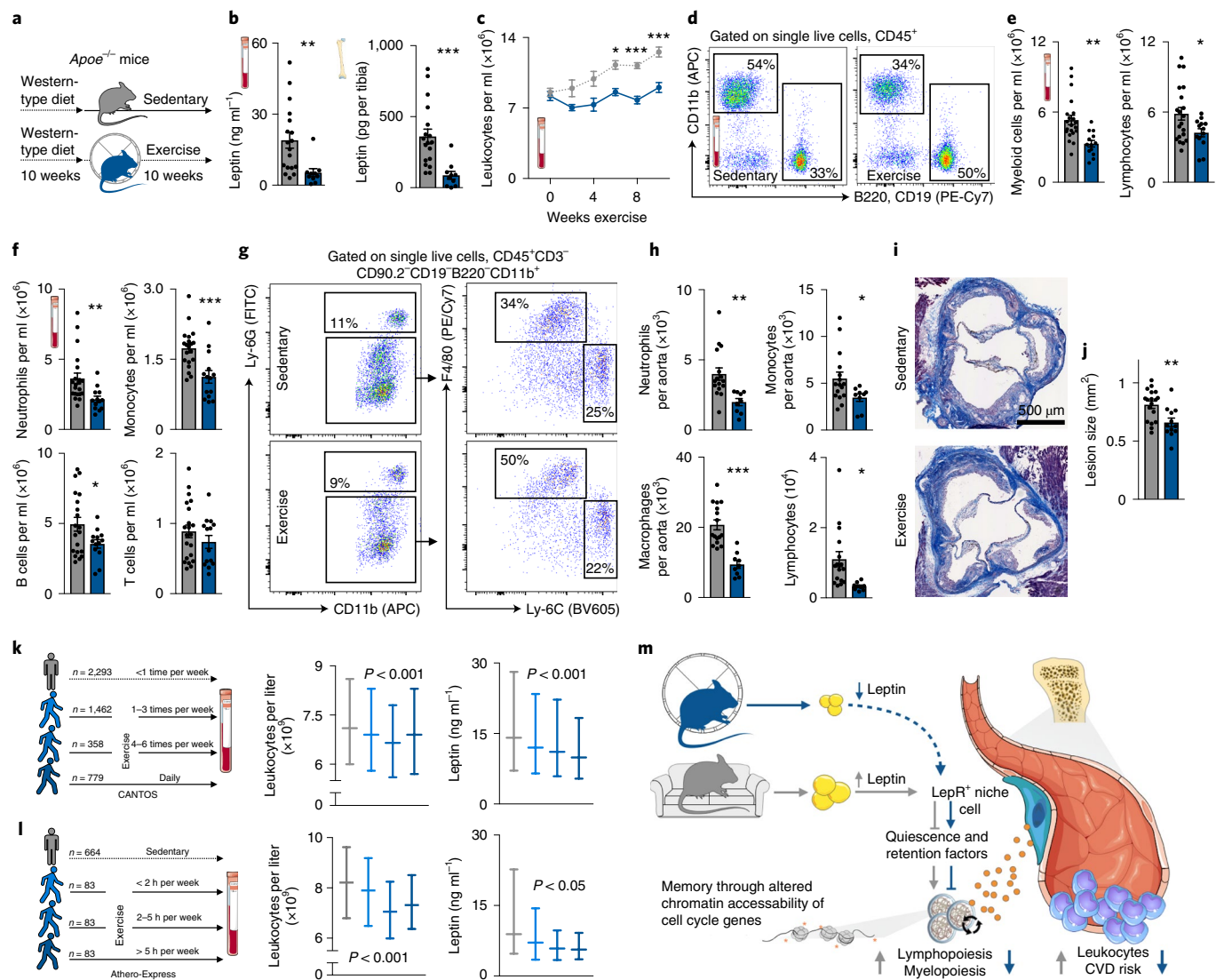


Fig. 6 | Sedentary lifestyle accelerates leukocyte supply in mice and humans with atherosclerosis. **a**, Experimental outline for **b–j**. Apoe^{-/-} mice consumed a Western-type diet for a total of 20 weeks. After 10 weeks, half of them were given access to a running wheel for 10 weeks. **b**, Leptin concentration in blood (**P=0.0011) and tibia (**P=4.06×10⁻⁵; n=18 animals for sedentary and n=10 animals for exercise; four independent experiments were conducted; data were analyzed by two-tailed Mann-Whitney U-test). **c**, Circulating leukocytes, as measured by flow cytometry, during the last 10 weeks of diet (*P=0.017, ***P=1.9×10⁻⁷ for 8 weeks, ***P=6×10⁻⁸ for 10 weeks; n=19 and n=13 animals for week 0, n=4 and n=5 animals for week 2, n=20 and n=14 animals for week 8, n=21 and n=14 animals for week 10, for sedentary and exercise, respectively, n=5 per group for week 4, n=7 per group for week 6; data were analyzed by two-way ANOVA with Sidak's post hoc test). **d**, Flow cytometry gating strategy for leukocytes. **e**, Blood myeloid cells (**P=0.0011; n=21 animals for sedentary and n=13 animals for exercise) and lymphocytes (*P=0.034; n=20 animals for sedentary and n=13 animals for exercise) in circulation (four independent experiments were conducted; data were analyzed by two-tailed Student's t-test). **f**, Neutrophils (**P=0.069; n=21 animals for sedentary and n=13 animals for exercise), monocytes (**P=0.00058; n=20 animals for sedentary and n=14 animals for exercise), B cells (*P=0.042; n=20 animals for sedentary and n=13 animals for exercise) and T cells (n=21 animals for sedentary and n=14 animals for exercise) in circulation (four independent experiments were conducted; data were analyzed by two-tailed Mann-Whitney U-test). **g,h**, Flow cytometry gating in aorta (**g**) and enumeration of neutrophils (**P=0.0036), monocytes (*P=0.046), macrophages (**P=1.88×10⁻⁵) and lymphocytes (*P=0.015, n=16 animals for sedentary and n=9 animals for exercise; two-tailed Student's t-test) (**h**). **i,j**, Masson's trichrome histology images of aortic root (**i**) for plaque size analysis (**j**) (**P=0.0043; n=18 animals for sedentary and n=12 animals for exercise; data were analyzed by two-tailed Student's t-test). Data are mean±s.e.m. **k**, Left, cohorts and numbers among 4,892 participants in CANTOS according to self-reported exercise level. Right, median values and interquartile ranges for leptin and the total leukocyte count according to exercise level. Effects were statistically significant across exercise groups for both leptin and leukocyte count in both univariate and multivariate models. **l**, Left, cohorts and numbers of patients from the Athero-Express study according to exercise level. Right, median values and interquartile ranges for leptin and total leucocyte count (see Extended Data Fig. 10i and Supplementary Tables 3–5); data were analyzed by one-way ANOVA and multivariate linear regression models with correction for age, sex, body mass index, diabetes, hypercholesterolemia and statin use. **m**, Summary cartoon; see text for details. We acknowledge Servier Medical Art (<https://smart.servier.com>) for providing images of mice and cartoon components.

reported data²⁴ obtained in mice with constitutive LepR knockout in stromal cells. In line with this notion, 2 weeks after tamoxifen injections, we did not observe the effects on osteogenesis (Extended

Data Fig. 6k,l) previously described in mice with constitutive LepR deficiency²⁴. We conclude that reduced leptin signaling leads to increased production of quiescence-promoting niche factors by

LepR⁺ stromal cells, which in turn lowers HSPC proliferation and leukocyte output.

Voluntary running reduces LSK chromatin accessibility. To explore how long the effects of exercise persist, we provided mice with running wheels for 6 weeks followed by 3 weeks of running wheel withdrawal (post-exercise sedentary group; Fig. 3a). Although running-induced leptin reduction and effects on hematopoietic niche factors waned in this cohort (Extended Data Fig. 7a–c), circulating leukocytes remained lower than in sedentary mice (Fig. 3b). By 6 weeks after cessation of running, the exercise effects on LSK proliferation and blood leukocytes vanished completely (Extended Data Fig. 7d,e). These observations suggest that adaptations to exercise convey short-term memory effects in hematopoietic cells. To test this hypothesis, we transplanted LSKs obtained from CD45.1^{STEM} (ref. 25) sedentary and CD45.2 exercising mice in a 1:1 ratio into irradiated sedentary *Ubc*-GFP recipients (Fig. 3c). In agreement with the quiescent LSK phenotype in exercising mice, LSKs obtained from sedentary donors contributed 1.8-fold more circulating leukocytes than those from exercising donors (Fig. 3d,e), even though LSKs from the two donors engrafted equally (Fig. 3f). LSKs derived from running mice proliferated less after transplantation into sedentary recipients, while LT-HSC numbers were similar (Fig. 3g). Competitive LSK transplantation from sedentary versus post-exercise sedentary donors showed equal contribution to blood leukocytes, whereas competition of LSKs from exercising versus post-exercise sedentary mice led to a transitional result (Extended Data Fig. 7f).

These data indicate that the effects of exercise on HSPCs last several weeks longer than those on leptin, LepR⁺ stromal cells and the niche factors produced by them. To test whether exercise memory in hematopoietic cells arises from epigenetic alterations, we performed an assay for transposase-accessible chromatin using sequencing (ATAC-seq) on LSKs sorted from sedentary, exercising and post-exercise sedentary cohorts (Fig. 3h). Most ATAC-seq peaks in LSKs mapped to promoter regions (Fig. 3i) in close proximity to transcriptional start sites (TSSs; Fig. 3j). Overall chromatin accessibility at promoters was reduced in LSKs from exercising mice compared to sedentary mice (Fig. 3j), whereas the background signal was comparable in all groups excluding experimental bias (Extended Data Fig. 8a). The reduced chromatin accessibility of LSKs was maintained in mice that had stopped exercising (Fig. 3j). Comparing LSKs from different activity groups revealed that chromatin proximal to 2,480 genes was significantly less accessible following exercise, whereas only 12 genes were more accessible (false discovery rate (FDR)<0.01; Fig. 3k–m, Extended Data Fig. 8b and Supplementary Table 1). The reduced chromatin accessibility in LSKs persisted in post-exercise sedentary mice (Fig. 3k–m and Extended Data Fig. 8c–e). Pathway enrichment analysis revealed that the genes with significantly reduced chromatin accessibility in LSKs following exercise are involved in transcription and cell cycle regulation (Fig. 3n). Similarly to LSKs in exercising mice, LSKs from post-exercise sedentary mice showed reduced accessibility among genes involved in cell cycle, nucleosome organization and mRNA processing (Extended Data Fig. 8d). Several genes involved in proliferation, myelopoiesis and B lymphopoiesis were significantly less accessible in LSKs of exercising and post-exercise sedentary mice (Fig. 3k–n, Extended Data Fig. 8c–e and Supplementary Table 1). Therefore, voluntary exercise induces alterations in the LSK epigenome that suppress accessibility and expression of genes involved in HSPC proliferation and lineage fate decisions. Not only are these changes maintained 3 weeks following running wheel withdrawal, but they also functionally translate to the observed effects of exercise on hematopoiesis and circulating leukocytes.

We complemented ATAC-seq with RNA-seq in LSKs sorted from the bone marrow of sedentary, exercising and post-exercise sedentary cohorts (see Supplementary Table 2 for differentially

expressed genes). A direct comparison of individual genes that scored in ATAC-seq as being less accessible after exercise with genes whose transcripts declined did not reach formal significance. This result is not unexpected, as a lack of direct overlap between chromatin accessibility and differential expression on the single-gene level has been reported previously²⁶. Moreover, it has been shown that establishment of chromatin architecture in mouse and human HSPCs reveals the differential potential of progeny before the execution of an RNA transcriptional program^{27–29}. Nonetheless, similar biological themes did emerge from our ATAC-seq and RNA-seq data analysis, reflecting heightened hematopoiesis in sedentary mice, which was reduced by voluntary exercise and maintained for a period following exercise withdrawal. Gene set enrichment analysis (GSEA) revealed a significant downregulation of the ‘Reactome cell cycle’ gene set in LSKs of exercising mice. Specifically, the Reactome cell cycle gene set was the second most significantly downregulated gene set (out of 410 Reactome gene sets) in exercising mice (FDR=0.004), was 49 out of 410 in post-exercise sedentary mice (FDR=0.01, likely reflecting the gradual return of these mice to a sedentary state) and, when both of these groups were jointly compared to sedentary mice, 13 out of 410 (FDR=0; Fig. 3o). Gene Ontology (GO) biological process categories featuring immune activation, including phagocytosis, complement activation and several immune responses (Fig. 3p), were enriched in downregulated genes of exercising and post-exercise sedentary mice. Reactome gene sets enriched in downregulated genes of exercising mice included G-protein-coupled receptor signaling (Fig. 3q). These receptors are critically involved in regulating HSPC retention, migration, proliferation and lineage bias³⁰. Finally, GSEA documented a metabolic switch from glycolysis in LSKs from exercising mice toward oxidative phosphorylation in sedentary mice (Fig. 3r), which typically occurs if HSPCs transition from quiescence toward proliferation³¹.

Exercise augments emergency hematopoiesis and improves survival in sepsis. Given our finding that exercise reduces circulating leukocytes and that clearance of infections relies on swift leukocyte supply, we wondered whether relative leukopenia exposes the host to a greater risk from infections, as described after acute exercise^{32,33}. To explore whether physical activity alters emergency hematopoiesis, we challenged mice with intraperitoneal injections of lipopolysaccharide (LPS), a bacterial cell wall component that induces inflammatory responses in sepsis. The hematopoietic progenitors of exercising mice responded vigorously, with a 1.4-fold increase of c.f.u. compared to progenitors from sedentary littermates (Fig. 4a,b). Higher HSPC numbers (Fig. 4c) gave rise to more neutrophils, monocytes, B cells and T cells in the blood and peritoneal cavity (Fig. 4d,e). When exposed to sepsis after cecal ligation and puncture, exercising mice had significantly lower mortality than sedentary mice (Fig. 4f–h). These findings, together with the earlier observation that exercise increases macrophage inflammatory cytokine production³⁴, argue against a compromised immune response in individuals that exercise regularly and indicate that exercise does not inhibit emergency hematopoiesis in the setting of infection.

Leptin receptor deletion dampens infarct inflammation. In CVD, emergency hematopoiesis is triggered by organ ischemia; we therefore studied how exercise influences the hematopoietic response after acute MI. Leptin increases in the blood of patients^{35,36} and in the blood and tibia of mice with MI (Fig. 5a). On day 6 after MI, leptin levels were comparable in exercising and sedentary mice (Extended Data Fig. 9a,b). Leukocyte numbers in the acute infarct did not change with exercise, and rose further with leptin supplementation by minipump (Extended Data Fig. 9c,d). Functional post-MI recovery was similar between sedentary and exercising mice (Extended Data Fig. 9e). Disrupting post-MI leptin sensing by stromal bone marrow niche cells in *Prrx1*-creER^{T2}; *Lepr*^{dfl} mice augmented production of hematopoietic niche

factors and reduced LSK proliferation in comparison to control *Lepr^{fl/fl}* mice (Fig. 5b–d). Bone marrow isolated from *Prrx1*-creER^{T2}; *Lepr^{fl/fl}* mice after MI gave rise to fewer colonies (Fig. 5e). As a result of blunted post-MI emergency hematopoiesis, systemic and cardiac leukocyte numbers were lower in *Prrx1*-creER^{T2}; *Lepr^{fl/fl}* mice (Fig. 5f,g). Such dampening of emergency hematopoiesis was replicated by treatment with leptin-neutralizing antibody 30 min after MI, which decreased bone marrow c.f.u., granulocyte-macrophage progenitor (GMP) proliferation and monocytes in the blood and infarct (Extended Data Fig. 9f–j). In accordance with clinical data correlating post-MI leukocyte levels with heart failure severity³⁷ and post-MI outcomes³⁸, reduced leukocytosis in *Prrx1*-creER^{T2}; *Lepr^{fl/fl}* mice improved recovery and reduced heart failure post-MI, as indicated by lower ventricular volumes and preserved ejection fraction measured by magnetic resonance imaging 3 weeks after MI (Fig. 5h–j). Histological analyses of the infarct border zone 7 d after MI indicated that this improved recovery was due to faster resolution of inflammation and reduced fibrosis (Extended Data Fig. 9k,l). Taken together, these data indicate that exercise does not inhibit emergency hematopoiesis after acute MI; however, disruption of leptin signaling by deleting its receptor exerts beneficial effects on post-MI recovery via dampening of leukocyte supply to the heart.

Sedentary lifestyle accelerates leukocyte supply in mice and patients with atherosclerosis. Systemic leukocyte availability correlates with atherosclerosis severity in mice³⁹ and humans³, exercise prevents atherosclerotic plaque initiation¹³ and progression^{14,15}, and a sedentary lifestyle associates strongly with cardiovascular risk. Because we found that physical activity in healthy mice influences leukocyte supply, we hypothesized that exercise, at least to some extent, affects atherosclerosis via dampening of leukocyte production and plaque inflammation. We thus gave *Apoe^{-/-}* mice with established atherosclerosis access to running wheels, which significantly reduced blood and tibial leptin concentration, inhibited progression of hyperlipidemia-associated leukocytosis, lowered immune cell accumulation in the aorta and decreased the size of atherosclerotic plaques in the aortic root (Fig. 6a–j). To examine the role of leptin in atherosclerosis mechanistically, we induced atherosclerosis in *Prrx1*-creER^{T2}; *Lepr^{fl/fl}* mice using a combination of atherogenic diet and PCSK9-encoding adeno-associated virus (AAV). Compared to littermate *Lepr^{fl/fl}* controls, deletion of LepR resulted in reduced atherosclerotic plaque size and macrophage content (Extended Data Fig. 10a–d). Mechanistically, this was tied to lower HSC and GMP proliferation and reduced circulating neutrophils and monocytes (Extended Data Fig. 10e–h). Of note, in contrast to mice without atherosclerosis, we observed exercise effects even on the level of CD48-CD150⁺ LT-HSCs, possibly because of the combined effects of hyperlipidemia, atherosclerosis and sedentary behavior.

These observations raised the question of whether exercise also has beneficial effects on hematopoiesis in patients with existing CVD. We assessed the association between self-reported exercise and plasma leptin levels or the total white blood cell count measured at baseline among 4,892 participants in CANTOS, which enrolled individuals who had sustained an MI (ref. ²). Plasma levels of leptin and the total leukocyte count were lower among CANTOS participants who exercised four or more times per week as compared to those with lower exercise levels ($P < 0.001$ in both univariate and multivariate analyses, Fig. 6k). Patients with CVD enrolled in the Athero-Express study⁴⁰ showed a similar relationship between blood leukocyte numbers, leptin and physical activity, even when correcting for age, sex, body mass index, smoking, diabetes, hypercholesterolemia and statin use (Fig. 6l, Extended Data Fig. 10i and Supplementary Tables 3–5). The association observed in two independent clinical cohorts, viewed together with the data obtained in mice, indicates that physical activity exerts beneficial effects on leptin and leukocytosis in patients with CVD.

Discussion

Our preclinical data show that voluntary physical activity protects against CVD via reduced chronic hematopoietic output of inflammatory leukocytes, due to diminished leptin signaling to the stromal hematopoietic bone marrow niche (Fig. 6m). Leptin levels increase when energy is abundant⁴¹. The hormone's role in regulating energetically costly hematopoiesis may have evolved to produce blood cells at times of resource sufficiency. However, contemporary sedentary behavior, which increases leptin and consequently hematopoiesis, may have rendered this adaptation a risk factor for CVD, and perhaps also for other diseases with inflammatory components.

The leukocyte reduction in voluntarily running mice contrasts sharply with the increased hematopoiesis, increased cell mobilization from the bone marrow and leukocytosis reported for forced endurance training^{42–45}. This difference may arise from exercise intensity and the stressful electric shocks used to enforce running^{42,45}. Such stress may activate sympathetic signaling and consequently accelerate HSPC proliferation⁶.

The associations between sedentary lifestyle, leptin and leukocyte levels in the two independent, large cardiovascular patient cohorts we describe here extend previous human data^{20,21,46,47} and support the clinical relevance of the pathways we target in sedentary mice. In agreement with these clinical data, leukocytosis and plaque size increase in sedentary mice with established atherosclerosis. The observed health benefits of physical activity are likely multifactorial and not limited to leptin-dependent regulation of hematopoiesis. Because exercise improves sepsis survival in mice, molecular alterations produced by voluntary running may inform anti-inflammatory drug discovery by identification of targets that do not compromise host defenses.

The insight that regular voluntary physical activity reduces hematopoiesis illuminates a new pathway by which sedentary lifestyle contributes to cardiovascular risk via oversupply of disease-promoting leukocytes. These data also support the notion that physical activity lessens existing chronic inflammation. Implementing guidelines⁴⁸ that recommend 150 min of exercise per week and development of drugs that mimic the effects of voluntary exercise on hematopoiesis offer modalities to mitigate inflammation in CVD.

Online content

Any methods, additional references, Nature Research reporting summaries, source data, extended data, supplementary information, acknowledgements, peer review information; details of author contributions and competing interests; and statements of data and code availability are available at <https://doi.org/10.1038/s41591-019-0633-x>.

Received: 18 May 2018; Accepted: 30 September 2019;

Published online: 07 November 2019

References

- Ridker, P. M. Residual inflammatory risk: addressing the obverse side of the atherosclerosis prevention coin. *Eur. Heart J.* **37**, 1720–1722 (2016).
- Ridker, P. M. et al. Anti-inflammatory therapy with canakinumab for atherosclerotic disease. *N. Engl. J. Med.* **377**, 1119–1131 (2017).
- Madjid, M., Awan, I., Willerson, J. T. & Casscells, S. W. Leukocyte count and coronary heart disease: implications for risk assessment. *J. Am. Coll. Cardiol.* **44**, 1945–1956 (2004).
- Nahrendorf, M. & Swirski, F. K. Lifestyle effects on hematopoiesis and atherosclerosis. *Circ. Res.* **116**, 884–894 (2015).
- Tall, A. R. & Yvan-Charvet, L. Cholesterol, inflammation and innate immunity. *Nat. Rev. Immunol.* **15**, 104–116 (2015).
- Heidt, T. et al. Chronic variable stress activates hematopoietic stem cells. *Nat. Med.* **20**, 754–758 (2014).
- McAlpine, C. S. et al. Sleep modulates haematopoiesis and protects against atherosclerosis. *Nature* **566**, 383–387 (2019).
- Nagareddy, P. R. et al. Adipose tissue macrophages promote myelopoiesis and monocytosis in obesity. *Cell Metab.* **19**, 821–835 (2014).
- Morrison, S. J. & Scadden, D. T. The bone marrow niche for haematopoietic stem cells. *Nature* **505**, 327–334 (2014).

10. Lavie, C. J., Ozemek, C., Carbone, S., Katzmarzyk, P. T. & Blair, S. N. Sedentary behavior, exercise, and cardiovascular health. *Circ. Res.* **124**, 799–815 (2019).
11. Lee, D. C. et al. Leisure-time running reduces all-cause and cardiovascular mortality risk. *J. Am. Coll. Cardiol.* **64**, 472–481 (2014).
12. Duggal, N. A., Niemiro, G., Harridge, S. D. R., Simpson, R. J. & Lord, J. M. Can physical activity ameliorate immunosenescence and thereby reduce age-related multi-morbidity? *Nat. Rev. Immunol.* **19**, 563–572 (2019).
13. Meissner, M. et al. Voluntary wheel running increases bile acid as well as cholesterol excretion and decreases atherosclerosis in hypercholesterolemic mice. *Atherosclerosis* **218**, 323–329 (2011).
14. Fukao, K. et al. Voluntary exercise ameliorates the progression of atherosclerotic lesion formation via anti-inflammatory effects in apolipoprotein E-deficient mice. *J. Atheroscler. Thromb.* **17**, 1226–1236 (2010).
15. Pellegrin, M. et al. Long-term exercise stabilizes atherosclerotic plaque in ApoE knockout mice. *Med. Sci. Sports Exerc.* **41**, 2128–2135 (2009).
16. de Visser, L., van den Bos, R. & Spruijt, B. M. Automated home cage observations as a tool to measure the effects of wheel running on cage floor locomotion. *Behav. Brain Res.* **160**, 382–388 (2005).
17. Asada, N., Takeishi, S. & Frenette, P. S. Complexity of bone marrow hematopoietic stem cell niche. *Int. J. Hematol.* **106**, 45–54 (2017).
18. Abella, V. et al. Leptin in the interplay of inflammation, metabolism and immune system disorders. *Nat. Rev. Rheumatol.* **13**, 100–109 (2017).
19. Bennett, B. D. et al. A role for leptin and its cognate receptor in hematopoiesis. *Curr. Biol.* **6**, 1170–1180 (1996).
20. Hirose, H. et al. Serum leptin level: possible association with haematopoiesis in adolescents, independent of body mass index and serum insulin. *Clin. Sci.* **94**, 633–636 (1998).
21. Rostas, I. et al. In middle-aged and old obese patients, training intervention reduces leptin level: a meta-analysis. *PLoS ONE* **12**, e0182801 (2017).
22. Zhou, B. O., Yue, R., Murphy, M. M., Peyer, J. G. & Morrison, S. J. Leptin-receptor-expressing mesenchymal stromal cells represent the main source of bone formed by adult bone marrow. *Cell Stem Cell* **15**, 154–168 (2014).
23. Ding, L., Saunders, T. L., Enikolopov, G. & Morrison, S. J. Endothelial and perivascular cells maintain haematopoietic stem cells. *Nature* **481**, 457–462 (2012).
24. Yue, R., Zhou, B. O., Shimada, I. S., Zhao, Z. & Morrison, S. J. Leptin receptor promotes adipogenesis and reduces osteogenesis by regulating mesenchymal stromal cells in adult bone marrow. *Cell Stem Cell* **18**, 782–96 (2016).
25. Mercier, F. E., Sykes, D. B. & Scadden, D. T. Single targeted exon mutation creates a true congenic mouse for competitive hematopoietic stem cell transplantation: the C57BL/6-CD45.1^{STEM} mouse. *Stem Cell Rep.* **6**, 985–992 (2016).
26. Cao, J. et al. Joint profiling of chromatin accessibility and gene expression in thousands of single cells. *Science* **361**, 1380–1385 (2018).
27. Lara-Astiaso, D. et al. Chromatin state dynamics during blood formation. *Science* **345**, 943–949 (2014).
28. Corces, M. R. et al. Lineage-specific and single-cell chromatin accessibility charts human hematopoiesis and leukemia evolution. *Nat. Genet.* **48**, 1193–1203 (2016).
29. Yu, V. W. C. et al. Epigenetic memory underlies cell-autonomous heterogeneous behavior of hematopoietic stem cells. *Cell* **167**, 1310–1322 (2016).
30. Golani, K., Kollet, O. & Lapidot, T. Dynamic cross talk between S1P and CXCL12 regulates hematopoietic stem cells migration, development and bone remodeling. *Pharmaceuticals* **6**, 1145–1169 (2013).
31. Ito, K. & Suda, T. Metabolic requirements for the maintenance of self-renewing stem cells. *Nat. Rev. Mol. Cell Biol.* **15**, 243–256 (2014).
32. Tanaka, Y. et al. Exhaustive exercise reduces tumor necrosis factor-alpha production in response to lipopolysaccharide in mice. *Neuroimmunomodulation* **17**, 279–286 (2010).
33. Mackinnon, L. T., Chick, T. W., van As, A. & Tomasi, T. B. The effect of exercise on secretory and natural immunity. *Adv. Exp. Med. Biol.* **216A**, 869–876 (1987).
34. Shirato, K. et al. Regular voluntary exercise potentiates interleukin-1 β and interleukin-18 secretion by increasing caspase-1 expression in murine macrophages. *Mediators Inflamm.* **2017**, 9290416 (2017).
35. Wallerstedt, S. M., Eriksson, A. L., Niklason, A., Ohlsson, C. & Hedner, T. Serum leptin and myocardial infarction in hypertension. *Blood Press.* **13**, 243–246 (2004).
36. Rajendran, K., Devarajan, N., Ganesan, M. & Ragunathan, M. Obesity, inflammation and acute myocardial infarction—expression of leptin, IL-6 and high sensitivity-CRP in a Chennai-based population. *Thromb. J.* **10**, 13 (2012).
37. Engström, G., Melander, O. & Hedblad, B. Leukocyte count and incidence of hospitalizations due to heart failure. *Circ. Heart Fail.* **2**, 217–222 (2009).
38. Tsujikawa, H. et al. Impact of heterogeneity of human peripheral blood monocyte subsets on myocardial salvage in patients with primary acute myocardial infarction. *J. Am. Coll. Cardiol.* **54**, 130–138 (2009).
39. Swirski, F. K. & Nahrendorf, M. Leukocyte behavior in atherosclerosis, myocardial infarction, and heart failure. *Science* **339**, 161–166 (2013).
40. Verhoeven, B. A. et al. Athero-Express: differential atherosclerotic plaque expression of mRNA and protein in relation to cardiovascular events and patient characteristics. Rationale and design. *Eur. J. Epidemiol.* **19**, 1127–1133 (2004).
41. Kelesidis, T., Kelesidis, I., Chou, S. & Mantzoros, C. S. Narrative review: the role of leptin in human physiology: emerging clinical applications. *Ann. Intern. Med.* **152**, 93–100 (2010).
42. De Lisio, M. & Parise, G. Characterization of the effects of exercise training on hematopoietic stem cell quantity and function. *J. Appl. Physiol.* **113**, 1576–1584 (2012).
43. Baker, J. M., De Lisio, M. & Parise, G. Endurance exercise training promotes medullary hematopoiesis. *FASEB J.* **25**, 4348–4357 (2011).
44. Agha, N. H. et al. Vigorous exercise mobilizes CD34 $^{+}$ hematopoietic stem cells to peripheral blood via the β_{2} -adrenergic receptor. *Brain Behav. Immun.* **68**, 66–75 (2018).
45. Soppi, E., Varjo, P., Eskola, J. & Laitinen, L. A. Effect of strenuous physical stress on circulating lymphocyte number and function before and after training. *J. Clin. Lab. Immunol.* **8**, 43–46 (1982).
46. Johannsen, N. M. et al. Effect of different doses of aerobic exercise on total white blood cell (WBC) and WBC subtraction number in postmenopausal women: results from DREW. *PLoS ONE* **7**, e31319 (2012).
47. Mabuchi, T. et al. Association between serum leptin concentration and white blood cell count in middle-aged Japanese men and women. *Diabetes Metab. Res. Rev.* **21**, 441–447 (2005).
48. Arnett, D. K. et al. 2019 ACC/AHA guideline on the primary prevention of cardiovascular disease: executive summary: a report of the American College of Cardiology/American Heart Association Task Force on clinical practice guidelines. *J. Am. Coll. Cardiol.* **74**, 1376–1414 (2019).

Publisher's note Springer Nature remains neutral with regard to jurisdictional claims in published maps and institutional affiliations.

© The Author(s), under exclusive licence to Springer Nature America, Inc. 2019

Methods

CANTOS. We assessed for evidence of association between self-reported exercise and plasma levels of leptin or the total white blood cell count measured at baseline among 4,892 participants in CANTOS who had a history of MI and who were receiving aggressive secondary preventive care, including high-intensity statin therapy². Leptin levels (R&D Systems) and the total leucocyte count were evaluated in a central laboratory and exercise levels were categorized as rarely, 1 to 3 sessions per week, 4 to 6 sessions per week or daily. Tests for significance across exercise categories were evaluated in univariate analyses using the Kruskal-Wallis test, and multivariate regression analyses were used to determine effects after adjustment for age, sex, body mass index, education level, history of heart failure and hemoglobin A1c. The study protocol was approved at participating centers by the responsible institutional review board or ethics committee, as applicable in the 39 countries involved. Written informed consent was obtained from trial participants.

Athero-Express. All patients included in the present analysis were enrolled in the Athero-Express Biobank study^{10,49}. The study is an ongoing, longitudinal biobank that combines blood and atherosclerotic plaque specimens with baseline characteristics and 3-year follow-up data from patients undergoing surgical revascularization to treat carotid or iliofemoral stenosis. Patient characteristics were obtained through standardized preoperative questionnaires and preoperative admission charts. All patients underwent surgery between 2005 and 2016 in the University Medical Center Utrecht. Indication for surgery was based on international guidelines for carotid and peripheral surgical revascularization⁵⁰. This study was conducted in accordance with the Declaration of Helsinki and all patients provided written informed consent. Patients were first stratified into two groups based on the information provided in response to a question about whether they performed any exercise. Patients who did not perform any exercise were the reference group. To study dose-dependent effects of exercise, patients were further stratified into tertiles based on the number of hours exercised per week. A flowchart of the study design is provided in Extended Data Fig. 10i. Hematological measurements were obtained from the Utrecht Patient Orientated Database⁵¹. Hematological parameters were measured using the Abbott CELL-DYN Sapphire (Abbott Diagnostics)^{52,53}.

Leptin measurements were performed in 44 patients per exercise group on blood drawn before surgeries. A custom-built Leptin Human Magnetic Luminex Assay (standard curve 493–119,830 pg ml⁻¹, sensitivity 10.2 pg ml⁻¹, R&D Systems) was used in combination with the Bio-Plex Multiplex system (Bio-Rad). Analyses were performed according to the manufacturer's protocol. Patients with leptin levels that were below the detection limit of the assay ($n=2$) were excluded.

Patients were categorized into four exercise groups, based on hours of exercise per week. Differences in binary characteristics between the four groups were analyzed with Pearson's chi-squared test. Differences in continuous variables among the four groups were tested using one-way ANOVA. White blood cell counts were compared among groups using one-way ANOVA and multivariate linear regression models. Possible confounders were selected on the basis of differences in baseline characteristics among the four exercise groups, and association with the hematologic parameter of interest (P value <0.10). SPSS v.21.0 (SPSS) was used for all statistical analyses. The study protocol was approved by the medical ethics committee of the University Medical Center Utrecht.

Mice. Seven- to 8-week-old male C57BL/6J mice were used for exercise studies if not indicated otherwise. *Ubc*-GFP (C57BL/6-Tg(UBC-GFP)30Scha/J, 004353), CD45.1 (B6.SJL-Ptprc^bPepc^b/Boy, 002014) and *Apoe*^{−/−} (B6.129P2-Apoe^{tm1Unc}/J, 002052) mice were purchased from the Jackson Laboratory. Stromal cell reporter mice (*Nes*-GFP^{54,55}, *Lepr*-cre; *Rosa26*-YFP or *Lepr*-cre; *Rosa26*-tdTomato^{23,56} and *Bglap*-GFP^{topaz} (ref. ⁵⁷)), CD45.1^{STEM} mice²⁵ and *Prrx1*-creER^{T2} mice (B6.Cg-Tg(*Prrx1*-cre/ERT2)-EGFP)1Smkm/J; JAX, 029211) crossed with *Lepr*^{fl/fl} mice (B6.129P2-Lepr^{tm1Rck}/J; JAX, 008327) were bred in house. Genotyping for each strain was performed as described on the Jackson Laboratory website. For the *Nes*-GFP and *Bglap*-GFP^{topaz} mice, we used genotyping primers that specifically targeted the GFP construct (forward primer: 5'-CTGGTCGAGCTGGACGGCGACGTAAC-3'; reverse primer: 5'-ATTGATCGCGCTTCTCGTTGGGG-3'). For inducible deletion of LepR, we intraperitoneally administered 75 mg kg^{−1} tamoxifen (T5648, Sigma-Aldrich) dissolved in corn oil (C8267, Sigma-Aldrich), according to the Jackson Laboratory protocol, every second day for 5 d (three injections in total). In all experiments, littermate control mice were subjected to the same tamoxifen regimen.

For atherosclerosis experiments in *Lepr*^{fl/fl} and *Prrx1*-creER^{T2}; *Lepr*^{fl/fl} strains, mice received a single intravenous injection of AAV-PCSK9 (10¹² genome copies in 200 µl of PBS) 2 weeks after the initial tamoxifen injections as described previously⁵⁸. pAAV/D377Y-mPCSK9 was a gift from J. Bentzon (Addgene plasmid 58376; <http://n2t.net/addgene:58376>; RRID: Addgene_58376). Following AAV-PCSK9 injection, mice were placed on a high-fat diet (D12108C, Research Diets) and underwent single injections of 75 mg kg^{−1} tamoxifen at 4 and 8 weeks after the start of the high-fat diet.

All mice were housed in separate cages in a pathogen-free environment at the Massachusetts General Hospital animal facility and maintained on a 12-h light/12-h dark cycle with a room temperature of 22 ± 1 °C. Mice received standard

mouse chow and water ad libitum, except for *Apoe*^{−/−} mice, which consumed a Western-type diet (TD.88137, Teklad Custom Diets, Envigo), and mice subjected to intravenous AAV-PCSK9 injections, which were fed an atherogenic diet (D12108C, Research Diets). All experiments were approved by the Subcommittee on Animal Research Care at Massachusetts General Hospital. All efforts were made to minimize suffering. If not bred in-house, mice were acclimatized for 1–2 weeks before experiments. Mice were randomized to experimental groups; *Apoe*^{−/−} mice were randomized according to leukocyte blood levels and weight at the beginning of exercise. The analysis of the effect of exercise before CLP and MI, as well as the effect of leptin inhibition after MI, was conducted in a blinded fashion.

Voluntary running wheels. Mice were individually housed in cages with low-profile wireless running wheels (ENV-047, Med Associates) for 6 or 10 weeks. These open-surface running wheels enabled unobstructed running by mice with mini-osmotic pump implantations. Sedentary mice were housed singly without running wheels but received a similarly sized igloo for enrichment. We initially housed mice with fixed running wheels in our pilot study but did not find a significant difference to housing mice with igloos.

Sepsis induction. LPS (0.5 mg kg^{−1}, from *Escherichia coli* 055:B5, Sigma-Aldrich) was administered intraperitoneally to mice that either had or had not previously exercised for 6 weeks. CLP, a model for sepsis, was carried out as previously described⁵⁹. In brief, a small incision was made to open the peritoneal cavity under general anesthesia (1–2% isoflurane) and the cecum was exteriorized and ligated at ~30% of the cecum with a non-absorbable 7-0 suture. The distal end of the cecum was perforated using a 23-gauge needle, and a small amount of feces was extruded through the puncture. The cecum was relocated into the peritoneal cavity and the peritoneum was closed with sutures. Mice received buprenorphine before surgery and twice daily thereafter for the first 3 d. One milliliter of saline was administered intraperitoneally to alleviate fluid loss. Rectal temperature was measured by inserting a temperature sensor under anesthesia.

Myocardial infarction. For MI, thoracotomy was performed in the fourth left intercostal space. The left coronary artery was identified and permanently ligated with a monofilament nylon 8-0 suture. The thorax wound was then closed with sutures. Throughout the experiment, mice were intubated and ventilated with 2% isoflurane supplemented with oxygen. Anti-leptin antibody (AF498) or IgG isotype control antibody (AB-108-C, both R&D Systems) was administered at a concentration of 1 mg kg^{−1}, 30 min after coronary artery ligation. AF498 has previously been shown to block the binding of leptin to its receptor in C57BL/6J mice⁶⁰.

Osmotic minipump implantation. Osmotic pumps (model 2006, Alzet) were implanted subcutaneously via a small incision between the scapulae, under general anesthesia (1–2% isoflurane). Subcutaneous connective tissue was spread to create a pocket for the pump. After pump insertion, the wound was closed with sutures. Animals were given buprenorphine (0.1 mg kg^{−1} subcutaneously) before surgery and twice daily for the first 72 h after implantation. Experiments started 72 h after implantation to allow the pumping rate to reach a steady state and to avoid any effect of surgery on exercise motivation. Pump filling was performed according to the manufacturer's protocol. The rate of infusion was 0.15 µl h^{−1}, which delivered 0.3 mg kg^{−1} per day of leptin for a period of 6 weeks. This dose was previously shown to not affect locomotor activity, weight gain, food intake and insulin or glucose levels⁵¹. Recombinant leptin (498-OB, R&D Systems) was dissolved in saline for infusion. To verify delivery, serum leptin levels and residual pump volume were routinely confirmed at the end of the experiment.

Tissue processing. Peripheral blood was collected by retro-orbital bleeding using heparinized capillary tubes (BD Biosciences). For flow cytometry analysis, red blood cells were lysed with 1× red blood cell lysis buffer (BioLegend). Blood was sampled and analyzed by automated complete blood count for platelets, red blood cells, hemoglobin and hematocrit on the Element Ht5 Auto Hematology analyzer. For organ collection, mice were perfused through the left ventricle with 20 ml of ice-cold PBS.

Bone marrow for qPCR analysis and bone marrow plasma were isolated by centrifugation. The metaphysis of one end of the tibia was removed and the bone was spun with the 'open end' facing down at 6,000g. For bone marrow plasma, the bone marrow pellet of one tibia was resuspended in 100 µl of PBS and spun down again, and the supernatant was kept for ELISA at −80 °C. For qPCR analysis, bone marrow was stored in RLT buffer (Qiagen) at −80 °C for further analysis. For flow cytometry analysis, bone marrow from the femurs was flushed with FACS buffer (1× PBS supplemented with 0.5 % BSA). For the LSK and stromal cell sorts, we isolated bone marrow from all long bones and the pelvis. For stromal cell isolations, the bone marrow fraction was digested to isolate nestin⁺ and LepR⁺ cells, and the bone fraction was digested to isolate OCN⁺ and nestin⁺ cells. The bone marrow fraction was isolated by flushing the bone marrow plug with a syringe into PBS supplemented with 2% FBS. After the bone marrow plug sank to the bottom of the tube, the supernatant was removed and replaced by the digestion mix: 1 mg ml^{−1} collagenase IV (Sigma-Aldrich, C5138), 2 mg ml^{−1} dispase (Gibco

by Life Technology, 17105-041) and 5 $\mu\text{l ml}^{-1}$ DNase I (Thermo Scientific, 90083) in HBSS buffer (Gibco by Life Technology, 14025-092). The bone marrow plug was digested 3 \times 15 min at 37 °C, as previously described⁶². Bones without the bone marrow plug were crushed and then cut into small pieces on a 70- μm cell strainer. Cells were washed with PBS supplemented with 2% FBS, and the bone fraction was collected and digested with collagenase I (Stem Cell Technology, 07902), 2 mg ml^{-1} dispase and 5 $\mu\text{l ml}^{-1}$ DNase I for 45 min at 37 °C under agitation (120 r.p.m.).

Peritoneal cells were recovered by lavage with 10 ml of ice-cold PBS supplemented with 2 mM EDTA. Spleens were triturated and filtered through a 40- μm filter to obtain single-cell suspensions and red blood cells were lysed with 1 \times red blood cell lysis buffer (BioLegend). Visceral adipose tissue (VAT) was either snap-frozen for qPCR analysis or minced into small pieces and subjected to enzymatic digestion according to Orr et al.⁶³ for flow cytometry. Briefly, no more than 300 mg of VAT was subjected to enzymatic digestion in 1 ml of digestion mix (1 \times PBS supplemented with 0.5% BSA, 10 mM CaCl₂ and 4 mg ml^{-1} collagenase type II, Worthington Biochemical Corporation) for 20 min at 37 °C under agitation (200 r.p.m.). Infarct and border zone heart tissue and abdominal aortas were minced into small pieces and subjected to enzymatic digestion with 450 U ml^{-1} collagenase I (C0130), 125 U ml^{-1} collagenase XI (C7657), 60 U ml^{-1} DNase I (D5319) and 60 U ml^{-1} hyaluronidase (H3506, all Sigma-Aldrich) for 30 min at 37 °C under agitation (750 r.p.m.). Gastrocnemius muscle was minced into small pieces and subjected to enzymatic digestion with 5 mg ml^{-1} collagenase type II and 60 U ml^{-1} DNase I (Sigma, D5319) in PBS supplemented with 2 mg ml^{-1} glucose and 50 mM CaCl₂. All digested tissues were then triturated and filtered through 40- μm (heart, spleen and muscle) or 70- μm (VAT) nylon mesh (Falcon), washed and centrifuged to obtain single-cell suspensions.

Flow cytometry. All single-cell suspensions were stained at 4 °C in 300 μl of FACS buffer (1 \times PBS supplemented with 0.5% BSA). For HSPC staining, isolated bone marrow cells were first stained with biotin-conjugated anti-mouse antibodies directed against mouse hematopoietic lineage markers, including CD3 (100304, clone 145-2C11), CD4 (100404, clone GK1.5), CD8α (100704, clone 53-6.7), CD49b (108904, clone DX5), CD90.2 (105304, clone 30-H12), CD19 (115503, clone 6D5), B220 (103204, clone RA3-6B2), NK1.1 (108704, clone PK136), TER119 (116204, clone TER-119), CD11b (101204, clone M1/70), CD11c (117304, clone N418) and Gr1 (108404, clone RB6-8C5; all 1:300 dilution, BioLegend). This was followed by a second staining with antibodies for CD16/32-BV711 (101337, clone 93), CD34-FITC (553733, clone RAM34, 1:150 dilution, BD Biosciences), CD48-AF700 (103426, clone HM48-1), CD115-BV421 (135513, clone AFS98), CD150-PerCP/Cy5.5 (115922, clone TC15-12F12.2), c-kit-PE/Cy7 (105814, clone 2B8), Sca-1-BV605 (108133, clone D7) and streptavidin-APC/Cy7 (405208; all 1:300 dilution, BioLegend unless otherwise indicated). Where applicable, cells were further stained with BrdU-APC (1:50 dilution, 552598, BD Biosciences) and Ki-67-FITC (11-5698-82, clone SolA15, Thermo Fisher Scientific) following the corresponding manufacturer's staining protocols. For aortic and cardiac leukocyte staining, cells were first stained with PE-conjugated antibodies to mouse hematopoietic lineage markers, including B220 (103208, clone RA3-6B2), CD19 (115508, clone 6D5), CD3 (100206, clone 17A2) and CD90.2 (140308, clone 53-2.1), and for cardiac leukocytes additionally for CD49b (108908, clone DX5), CD103 (121406, clone 2E7), NK1.1 (108708, PK136) and Ter119 (116208, clone TER-119; all 1:300 dilution, BioLegend). This was followed by a second staining for CD11b-APC (101212, clone M1/70), CD45-BV711 (103147, clone 30-F11), F4/80-PECy7 (1:150, 123114, clone BM8), Ly-6C-BV605 (128035) and Ly-6G-FITC (127605; all 1:300 dilution unless indicated otherwise, BioLegend). For blood and bone marrow leukocyte staining, cells were stained with B220-PE/Cy7 (103222, clone RA3-6B2) or B220-APC/Cy7 (103224, clone RA3-6B2), CD3-PE (100206, clone 17A2), CD4-PerCP/Cy5.5 (100434, clone GK1.5), CD8α-BV711 (100748, clone 53-6.7), CD19-PE/Cy7 (115520, clone 6D5) or CD19-APC/Cy7 (115530, clone 6D5), CD45-BV711 (103147, clone 30-F11) or CD45.2-AF700 (109822, clone 104), CD90.2-PE (140308, clone 53-2.1), Ly-6C-BV605 (128035, clone HK1.4), Ly-6G-FITC (127605, clone 1A8), CD11b-APC (101212, clone M1/70), NK1.1-APC/Cy7 (108730, clone PK136, 1:300 dilution) and CD115-BV421 (135513, clone AFS98; all 1:600 dilution unless indicated otherwise, BioLegend). Blood and bone marrow leukocyte staining samples were fixed with BD Cytofix (BD Biosciences) and analyzed within 24 h.

All cells were routinely incubated with a viability dye (FxCycle Violet Stain, F10347 or LIVE/DEAD Fixable Aqua Dead Cell Stain kit for 405 nm excitation, L-34966, both Thermo Fisher Scientific, or 7-AAD, 559925, BD Biosciences) and anti-CD16/32 Fc block (553142, BD Biosciences; except HSPC staining), according to the manufacturer's protocol.

All cells were prepped on viable and single cells (FSC-A versus FSC-W and SSC-A versus SSC-W). LSKs were identified as Lin⁻c-kit⁺Sca-1⁺. These were further divided into LT-HSCs (Lin⁻c-kit⁺Sca-1⁺CD150⁺CD48⁻), ST-HSCs (Lin⁻c-Kit⁺Sca-1⁺CD150⁻CD48⁻) and MPPs (Lin⁻c-kit⁺Sca-1⁺CD150⁻CD48⁺). CMPs were identified as Lin⁻c-Kit⁺Sca-1⁺CD16/32^{mid}CD34⁺; megakaryocyte erythroid progenitors as Lin⁻c-kit⁺Sca-1⁺CD16/32⁻CD34⁺; GMPs as Lin⁻c-kit⁺Sca-1⁺CD16/32⁺CD34⁺; macrophages and MDPs as Lin⁻c-kit⁺Sca-1⁺CD16/32⁺CD34⁺CD115⁺ and B cell progenitors as Lin⁻IgM⁺IgD⁺B220⁺. Monocytes were identified as B220-CD3-CD19-CD90.2-NK1.1-Ly-

6G⁻SSC^{low}CD11b⁺CD115⁺; neutrophils as B220-CD3-CD19-CD90.2-NK1.1-CD115-SSC^{low}CD11b⁺Ly-6G⁺; NK cells as B220-CD3-CD19-CD90.2-CD115-Ly-6G⁻SSC^{low}CD11b⁺NK1.1⁺; eosinophils as B220-CD3-CD19-CD90.2-CD115-Ly-6G⁻NK1.1-CD11b⁺SSC^{hi}; B cells as CD3-CD90.2-CD11b⁻B220⁺CD19⁺; and CD3⁺ T cells as B220-CD19-CD11b⁻CD3⁺CD90.2⁺. CD3⁺ T cells were further subdivided into CD4⁺ and CD8⁺ T cells. Osteolineage (OCN⁺) cells were identified as CD45-Ter119-CD31-GFP⁺ cells from OCN-GFP mice. LepR⁺ cells were identified as CD45-Ter119-CD31-YFP⁺ or CD45-Ter119-CD31-tdTomato⁺ cells from *Lepr-cre*; *Rosa26-YFP* or *Lepr-cre*; *Rosa26-tdTomato* mice. Nestin⁺ cells were identified as CD45-Ter119-CD31-GFP⁺ cells from Nes-GFP mice. Endothelial cells were identified as CD45-Ter119-CD31-⁻ cells from the bone marrow fraction of Nes-GFP mice. For compensation, the aforementioned antibodies were conjugated to OneComp eBeads (01-1111-42, Affymetrix). Unstained, YFP⁺, GFP⁺ and tdTomato⁺ control samples were used for compensation and to control the gating strategy. All data were acquired on an LSRII (BD Biosciences) and analyzed with FlowJo software. See the Life Sciences Reporting Summary for additional information.

Cell sorting and transplantation. To purify bone marrow stromal cells, samples were stained with CD31-BUV737 (565097, BD Biosciences), CD45-APC/Cy7 (103116, BioLegend), Ter119- APC/Cy7 (560509, BD Biosciences) and 7-AAD (BD Biosciences) and were FACS-sorted with a FACSAria II cell sorter (BD Biosciences).

To purify LSKs, PE lineage depletion was performed with MACS columns (130-042-401, Miltenyi Biotec), according to the manufacturer's protocol. Briefly, single-cell suspensions were stained with a lineage cocktail of PE-conjugated antibodies to CD3 (100206, clone 17A2), CD4 (130310, clone H129.19), CD8 (100708, clone 53-6.7), CD49b (108908, clone DX5), CD90.2 (140308, clone 53-2.1), CD19 (115508, clone 6D5), B220 (103208, clone RA3-6B2), NK1.1 (108708, clone PK136), TER119 (116208, clone TER-119), CD11b (101208, clone M1/70), CD11c (117308, clone N418) and Gr1 (108408, clone RB6-8C5; all 1:150, BioLegend), followed by incubation with anti-PE microbeads (130-048-801, Miltenyi Biotec). Lineage-depleted bone marrow cells were then stained with CD48-AF700 (103426, clone HM48-1), CD150-PerCP/Cy5.5 (115922, clone TC15-12F12.2), c-kit-PE/Cy7 (105814, clone 2B8) and Sca-1-BV605 (108133, clone D7; all 1:150 dilution, all BioLegend) and FACS-sorted using a FACSAria II cell sorter (BD Biosciences).

All cells were prepped on single cells (as determined by FSC-A versus FSC-W, and SSC-A versus SSC-W) and viable cells (DAPI⁻ for LSKs and 7-AAD⁻ for stromal cells).

For bone marrow transplants, each lethally irradiated (9.5 Gy) recipient *Ubc*-GFP mouse received 5,000 LSKs of exercising CD45.2 C57BL/6J mice and 5,000 LSKs of sedentary CD45.1^{1ST} mice. Each recipient CD45.1^{1ST} mouse received 5,000 LSKs of post-exercise sedentary GFP mice and 5,000 LSKs of either sedentary or exercising CD45.2 C57BL/6J mice. Additionally, 500,000 bone marrow cells from a *Ubc*-GFP mouse or CD45.1^{1ST} mouse were transferred matching the recipient mouse. We used CD45.1^{1ST} mice for competitive transplantation because these are equivalent to CD45.2 C57BL/6J mice in competitive bone marrow transplantation assays⁵⁰.

Real-time PCR. Total RNA from tissues was extracted using the RNeasy Mini kit (74104, Qiagen) and from FACS-purified cells using the NucleoSpin RNA XS kit (740902.50, Takara Bio), according to the manufacturers' protocols. RNase-free DNase Set (79254, Qiagen) was used for DNase digestion during RNA purification. RNA quality was assessed by NanoDrop for RNA isolated from tissues and with the Agilent RNA 6000 Pico kit (5067-1513, Agilent Technologies) on the Agilent 2100 Bioanalyzer for RNA of FACS-purified cells. First-strand cDNA was synthesized using the High-Capacity RNA-to-cDNA kit (4387406, Applied Biosystems). TaqMan gene expression assays were used to quantify target genes, using TaqMan Fast Universal PCR Master Mix (4366072, Applied Biosystems) and primers for *Cxcl12* (Mm00445553_m1), *Vcam1* (Mm01320970_m1), *Kif1* (Mm00442972_m1), *Angpt1* (Mm00456503_m1), *Iil1b* (Mm00434228_m1), *Pf4* (Mm00451315_g1), *Cld1* (Mm00441242_m1), *Il6* (Mm00446190_m1), *Il7* (Mm01295803_m1), *Tgfb1* (Mm01178820_m1), *Csf1* (Mm00432686_m1), *Csf2* (Mm01290062_m1), *Csf3* (Mm00438334_m1), *Sp7* (Mm04209856_m1), *Bglap* (Mm03413826_mH), *Runx2* (Mm00501584_m1), *Lpl* (Mm00434764_m1), *Fabp4* (Mm00445878_m1), *Lep* (Mm00434759_m1) (all FAM probes, Applied Biosystems) and *Actb* (4352341E, VIC probe, Applied Biosystems). Samples were run on a 7500 thermal cycler (Applied Biosystems) and the relative changes were normalized to *Actb* mRNA using the 2^{-ΔΔCt} method and normalized to sedentary controls.

ATAC-seq. Sorted LSKs underwent ATAC-seq as previously described^{64,65}. Briefly, 20,000 sorted LSK cells were initially resuspended in lysis buffer and centrifuged. The nuclei pellets were then subjected to transposition reaction using the Nextera Tn5 transposase enzyme (Illumina). Tagmented DNA was purified with the MinElute PCR Purification kit and eluted in 10 μl of elution buffer (Qiagen). Barcoded libraries were prepared and PCR amplified. Double-sided bead purification was performed using AMPure XP beads to remove primer dimers and

large >1,000-bp fragments. Libraries were sequenced as 50-bp paired-end reads on an Illumina HiSeq 2500.

Sequencing reads were first mapped to the mm10 reference genome using BWA-MEM⁶⁶ with default parameters, followed by calling peaks using HOTSPOT2 (ref. ⁶⁷). As a result, at each time point, we identified 8,000–10,000 peaks, which showed high consistency between biological duplicates. The union of these peak sets (14,313 peaks in total) was used to calculate the ATAC-seq coverage over each peak region across all samples. Peaks with differential accessibility between conditions were identified using edgeR⁶⁸, with cutoffs of at least 1.5-fold difference in normalized read density and FDR < 0.01.

RNA-seq. LSKs were sorted and RNA was isolated as described above. Sequencing-ready cDNA libraries were prepared using the Takara SMART-Seq v.4 kit, paired with the NexteraXT Library Prep kit for Illumina, following the manufacturer's protocol. Bioanalyzer DNA High Sensitivity traces were used to confirm cDNA size distribution after the SMART-Seq step, and Agilent High Sensitivity D1000 Tapestation traces were used to check the final library size distribution. The libraries were quantified by real-time PCR using the KAPA Library Quantification kit, and then sequenced as single-end 75-bp reads on an Illumina NextSeq 500 in high-output mode.

Transcript abundance from RNA-seq reads was quantified by Salmon⁶⁹, and gene-level counts were obtained with tximport⁷⁰. Subsequently, raw counts were processed with edgeR⁷¹ to determine differentially expressed genes. GSEA was performed on gene lists ranked by the edgeR fold change. We used 1,000 gene set permutations and the classic enrichment statistic. Gene set collections were from MSigDB (<http://software.broadinstitute.org/gsea/msigdb>). Furthermore, we used the R package ClusterProfiler⁷² to determine GO and Reactome categories that were enriched in genes downregulated in exercising versus sedentary groups. Raw counts from the experiment are available at the Gene Expression Omnibus under the accession [GSE124799](#).

ELISA. For the leptin ELISA (MOB00, R&D Systems) measurements, blood plasma was diluted 20-fold and bone marrow plasma was diluted twofold. For the CXCL12 ELISA (ab100741, Abcam) measurements, bone marrow plasma was diluted fourfold. For corticosterone ELISA (ab108821, Abcam) measurements, blood plasma was diluted 500-fold. Samples were analyzed according to the manufacturers' instructions.

Histology. Tibiae were collected and fixed immediately in 15 ml of 10% formalin solution (HT501128, Sigma-Aldrich) overnight at 4°C. Tibiae were then washed with distilled water, decalcified in 0.5 M EDTA (BM-711, Boston BioProducts) for 3 d and placed in 70% ethanol before embedding in paraffin and processing. Paraffin-embedded sections were deparaffinized in xylene using two changes for 5 min each and rehydrated in gradually graded ethanol. For RUNX2 staining, antigen retrieval was performed with 20 µg ml⁻¹ proteinase K (P2308, Sigma-Aldrich) for 15 min at 37°C and endogenous peroxidase activity was blocked with 3% H₂O₂ in methanol for 20 min at room temperature. Sections were stained with anti-Runx2 antibody (1:200 dilution, 12556, Cell Signaling) followed by secondary goat anti-rabbit IgG antibody (1:500 dilution, BA-1000, Vector Laboratories). Further, the TSA biotin detection kit (NEL700A, Perkin Elmer) was used and slides were stained with the DAB peroxidase (HRP) substrate kit (SK-4100, Vector Laboratories). For perilipin staining, antigen retrieval was performed using Retrievagen A (pH 6.0; 550524, BD Biosciences) and sections were stained for perilipin A (1:500 dilution, P1998, Sigma-Aldrich) followed by a biotinylated goat anti-rabbit IgG antibody (1:100 dilution, BA-1000, Vector Laboratories). Streptavidin DyLight 594 (1:600 dilution, SA-5594, Vector Laboratories) was applied to detect adipocytes, and DAPI (1:3,000 dilution, D21490, Thermo Fisher Scientific) was used to identify nuclei.

Aortic roots were dissected and embedded in Tissue-Tek O.C.T. compound (4583, Sakura Finetek), frozen in 2-methylbutane (78-78-4, Fisher Scientific) cooled with dry ice and sectioned into 6-µm slices. To compare lesion size between groups, Masson's trichrome (HT15-1KT, Sigma-Aldrich) and Oil Red O (O0625, Sigma-Aldrich) staining was performed according to the manufacturer's protocols and maximum lesion areas were measured. To quantify lesion macrophage content, immunohistochemistry was performed with anti-CD68 antibody (1:50 dilution, clone FA-11, 137002, BioLegend), the Vectastain ABC kit (Vector Laboratories) and AEC substrate (Dako). Slides were counterstained with Harris hematoxylin (Sigma-Aldrich). Images were captured on a NanoZoomer 2.0RS (Hamamatsu, Japan). Hearts were collected and embedded in O.C.T. compound. The sections were stained for CD11b (1:25 dilution, clone M1/70, 550282, BD Biosciences), collagen I (1:50 dilution, ab21286, Abcam) and alpha smooth muscle actin (1:50 dilution, ab5694, Abcam). Biotinylated secondary antibodies were applied followed by the VECTASTAIN ABC kit (PK-6100, Vector Laboratories) and AEC substrate (K3464, Dako) for color development. Sections were counterstained with Harris hematoxylin (HHS32, Sigma-Aldrich). All slides were scanned by digital slide scanner, NanoZoomer 2.0RS (Hamamatsu), and quantification was performed using ImageJ software.

In vivo calcein labeling and calculation of mineral apposition rate. Mice were intraperitoneally injected with 20 mg kg⁻¹ calcein (C0875, Sigma-Aldrich)

7 d before collection and 30 mg kg⁻¹ Alizarin red S (A5533, Sigma-Aldrich) in a 2% sodium bicarbonate solution 2 d before collection. Femurs were fixed for 2 h in formalin at 4°C and then embedded in O.C.T. compound and sectioned. Images were acquired on an Olympus IV100 microscope and post-processing was performed using ImageJ software (National Institutes of Health). The mineral apposition rate was the distance between the midpoints of the two labels divided by the time between the midpoints of the interval.

In vitro adipocyte differentiation assay. The bone marrow fraction was isolated from all long bones and pelvic bones and digested as previously described. All cells were plated in α-MEM (SH30265.01, Fisher Scientific) supplemented with 10% FBS and 1% penicillin-streptomycin (both Sigma-Aldrich). Medium was changed after 24 h to remove non-adherent hematopoietic cells. Stromal cells were then plated onto 12-well plates at a concentration of 50 × 10³ cells per well in differentiation medium (α-MEM supplemented with 10% FBS, 1% penicillin-streptomycin, 100 nM dexamethasone and 10 mg ml⁻¹ human insulin (1285-014, Gibco)). The differentiation medium was changed twice a week, and at day 21 cells were fixed in 4% paraformaldehyde for 10 min, washed with 60% isopropanol and stained with Oil Red O (O0625, Sigma-Aldrich) for 10 min and immediately washed with distilled water. After taking pictures, we extracted the Oil Red O with 100% isopropanol for 5 min with gentle rocking and the absorbance measurement was performed at 492 nm. The 100% isopropanol was used as a background control to subtract the background signal.

Micro-computed tomography. A high-resolution desktop micro-computed tomography (µCT) imaging system (µCT40, Scanco Medical AG) was used to assess trabecular bone microarchitecture and cortical bone morphology, in the proximal metaphysis and diaphysis of the tibia, respectively. Scans were acquired using a 10 µm³ isotropic voxel size, 70-kVp peak X-ray tube potential, 114-µA X-ray intensity and 200-ms integration time and were subjected to Gaussian filtration and segmentation. Image acquisition and analysis protocols adhered to guidelines for µCT assessment of rodent bone microstructure⁷³. Trabecular bone microarchitecture was analyzed in a 1,000-µm-long (100 transverse slices) region that began 100 µm inferior to the proximal growth plate and extended distally. The endocortical region was manually contoured and then bone was segmented from soft tissue using a threshold of 345 mgHA cm⁻³. The segmented images were analyzed with the standard Scanco trabecular bone morphology script to measure trabecular bone volume fraction (%), trabecular bone mineral density (mgHA cm⁻³), trabecular thickness (mm), trabecular number (mm⁻¹) and trabecular separation (mm). Cortical bone morphology was analyzed in a 500-µm-long (50 transverse slices) region that began 2 mm superior to the distal tibiofibular junction and extended distally. Cortical bone was segmented using a threshold of 700 mgHA cm⁻³ and the standard Scanco script for cortical bone morphology was used to measure total cross-sectional area (mm²), cortical bone area (mm²), cortical thickness (Ct.Th, mm) and polar moments of inertia (mm⁴).

Osmium tetroxide µCT. Bone marrow adipose tissue (MAT) was quantified by osmium tetroxide staining followed by µCT using previously described methods⁷⁴. Following µCT scanning for trabecular and cortical structure, the tibiae were demineralized in 4.1% EDTA for 21 d. The demineralized tibiae were then stained at room temperature for 48 h in a solution containing 1% osmium tetroxide and 2.5% potassium dichromate. After being washed with cold water to remove unbound osmium tetroxide, the stained tibiae were imaged using the previously mentioned µCT scanner. Scans of the proximal tibia were acquired using a 10 µm³ isotropic voxel size, 55-kVp peak X-ray tube potential, 145-µA X-ray intensity and 300-ms integration time and were subjected to Gaussian filtration and segmentation. The medullary cavity for each tibia was manually contoured in a region beginning 100 µm distal to the proximal growth plate and extending distally 2 mm. Osmium tetroxide staining in this region was segmented using a threshold equivalent to 800 mgHA cm⁻³, and volumetric analysis was run to measure MAT volume (MAT.V, mm³). The medullary volume (MV, mm³) in this region was quantified in the µCT scans of the mineralized bone as total volume minus bone volume (MV = total volume – bone volume). MAT volume was normalized by the medullary volume and is reported as the MAT volume fraction (MAT.V/MV, %).

MRI. cMRI was performed 21 d after coronary ligation to assess left ventricular dilatation and ejection fraction. MRI short-axis views of the entire left ventricle were acquired on a Bruker 4.7 Tesla PhamaScan magnet (Billerica) with a cine fast low-angle shot sequence with intraGate technology using the following parameters: echo time: 2.945 ms; repetition time: 10.0 ms; flip angle: 18 degrees; oversampling: 250; frames: 16; matrix: 200 × 200 × 1; and voxel size: 0.150 × 0.150 × 1 mm. The left ventricular wall and cavity were segmented manually at systole and diastole using Horos software (<https://horosproject.org>).

Mass spectrometry. For analysis of norepinephrine (NE) and acetylcholine (ACh), bone marrow samples were homogenized in cold 10 mM NH₄COOH (pH 3) in 57% ACN with isotopic labeled internal standards (ACh-d4 and NE-d6). CHCl₃ was added to achieve CH₃CN:H₂O:CHCl₃ (2:1.5:1 dilution) to denature proteins, and the mixture was centrifuged for 20 min at 4°C for phase separation. The upper

phase was used for ultra-performance liquid chromatography (UPLC)–tandem mass spectrometry (MS/MS) analysis.

An ACQUITY UPLC H-Class system and a Xevo TQ-S micro triple-quadrupole mass spectrometer with an electrospray source (all from Waters) were used for UPLC–MS/MS analysis. Separation was performed on two types of columns. An Acquity UPLC HSS PFP (150 mm × 2.1 mm, 1.8 µm) column was used for analysis of NE with a binary gradient (Solvent A was 0.2% formic acid and solvent B was methanol) at a flow rate of 0.4 ml min⁻¹. An Acquity UPLC BEH HILIC (50 mm × 2.1 mm, 1.7 µm) column was used for analysis of ACh with a binary gradient (Solvent A was 50% ACN, 10 mM NH₄COOH (pH 3) and solvent B was 95% ACN, 10 mM NH₄COOH, pH 3) at a flow rate of 0.55 ml min⁻¹. Three multiple-reaction monitoring (MRM) transitions were set up for each analyte: one for quantification (ACh 146→87; NE 152→107), one for confirmation (ACh 146→43; NE 152→79), and one for labeled internal standard (ACh-d4 150→91; NE-d6 158→139). These MRM were scheduled around the retention time of the analytes. Optimized cone voltage and collision energy were used for each of the individual MRM. No fewer than 12 data points were collected for each peak.

Statistical analyses. All statistical analyses of mouse studies were conducted with GraphPad Prism Software v7.0c. Data are presented as mean ± s.e.m. The sample size for each experiment is reported in the text and figure legends. All experiments were performed at least in duplicate.

All data were first tested for normality by D'Agostino–Pearson omnibus normality test. To compare two groups of mice, we used a two-tailed Student's *t*-test to compare normally distributed data and a two-tailed Mann–Whitney *U*-test for non-normal distribution. To compare three groups of mice, the Kruskal–Wallis test with Dunn's post hoc test was used for non-normal distributions. To compare two groups of mice with analysis at different time points, a two-way ANOVA with Sidak's post hoc test was used. The Mantel–Cox log-rank test was performed to compare survival of sedentary versus exercising mice after CLP. *P*<0.05 was considered to denote significance. Statistical outliers (not more than one per experiment) were determined with the two-sided Grubbs' outlier test (GraphPad Software) and excluded.

Reporting Summary. Further information on research design is available in the Nature Research Reporting Summary linked to this article.

Data availability

All data are included in this published article and its supplementary information files. Raw sequencing data are available from Gene Expression Omnibus under accession numbers [GSE110639](#) and [GSE124799](#). Raw data other than sequencing data that support the findings of this study are available from the corresponding author upon reasonable request. Source data are available for Figs. 1–6.

References

49. Ionita, M. G. et al. High neutrophil numbers in human carotid atherosclerotic plaques are associated with characteristics of rupture-prone lesions. *Arterioscler. Thromb. Vasc. Biol.* **30**, 1842–1848 (2010).
50. Halliday, A. et al. Prevention of disabling and fatal strokes by successful carotid endarterectomy in patients without recent neurological symptoms: randomised controlled trial. *Lancet* **363**, 1491–1502 (2004).
51. ten Berg, M. J. et al. Linking laboratory and medication data: new opportunities for pharmacoepidemiological research. *Clin. Chem. Lab. Med.* **45**, 13–19 (2007).
52. Lam, S. W., Leenen, L. P. H., Solinge, W. W., Hietbrink, F. & Huisman, A. Evaluation of hematological parameters on admission for the prediction of 7-day in-hospital mortality in a large trauma cohort. *Clin. Chem. Lab. Med.* **49**, 493–499 (2011).
53. Groeneveld, K. M., Heeres, M., Leenen, L. P. H., Huisman, A. & Koenderman, L. Immunophenotyping of posttraumatic neutrophils on a routine haematology analyser. *Mediators Inflamm.* **2012**, 509513 (2012).
54. Mignone, J. L., Kukekov, V., Chiang, A. S., Steindler, D. & Enikolopov, G. Neural stem and progenitor cells in nestin-GFP transgenic mice. *J. Comp. Neurol.* **469**, 311–324 (2004).
55. Méndez-Ferrer, S. et al. Mesenchymal and haematopoietic stem cells form a unique bone marrow niche. *Nature* **466**, 829–834 (2010).
56. DeFalco, J. et al. Virus-assisted mapping of neural inputs to a feeding center in the hypothalamus. *Science* **291**, 2608–2613 (2001).
57. Bilic-Curcic, I. et al. Visualizing levels of osteoblast differentiation by a two-color promoter-GFP strategy: type I collagen-GFPcyan and osteocalcin-GFPptz. *Genesis* **43**, 87–98 (2005).
58. Bjorklund, M. M. et al. Induction of atherosclerosis in mice and hamsters without germline genetic engineering. *Circ. Res.* **114**, 1684–1689 (2014).
59. Rittirsch, D., Huber-Lang, M. S., Flierl, M. A. & Ward, P. A. Immunodesign of experimental sepsis by cecal ligation and puncture. *Nat. Protoc.* **4**, 31–36 (2008).
60. Konstantinides, S., Schäfer, K., Neels, J. G., Dellas, C. & Loskutoff, D. J. Inhibition of endogenous leptin protects mice from arterial and venous thrombosis. *Arterioscler. Thromb. Vasc. Biol.* **24**, 2196–2201 (2004).
61. Surwit, R. S., Edwards, C. L., Murthy, S. & Petro, A. E. Transient effects of long-term leptin supplementation in the prevention of diet-induced obesity in mice. *Diabetes* **49**, 1203–1208 (2000).
62. Kunisaki, Y. et al. Arteriolar niches maintain haematopoietic stem cell quiescence. *Nature* **502**, 637–643 (2013).
63. Orr, J. S., Kennedy, A. J. & Hasty, A. H. Isolation of adipose tissue immune cells. *J. Vis. Exp.* **22**, e50707 (2013).
64. Buenrostro, J. D., Wu, B., Chang, H. Y. & Greenleaf, W. J. ATAC-seq: a method for assaying chromatin accessibility genome-wide. *Curr. Protoc. Mol. Biol.* **109**, 1–9 (2015).
65. Mehta, S. et al. Maintenance of macrophage transcriptional programs and intestinal homeostasis by epigenetic reader SP140. *Sci. Immunol.* **2**, eaag3160 (2017).
66. Li, H. Exploring single-sample SNP and INDEL calling with whole-genome de novo assembly. *Bioinformatics* **28**, 1838–1844 (2012).
67. John, S. et al. Chromatin accessibility pre-determines glucocorticoid receptor binding patterns. *Nat. Genet.* **43**, 264–268 (2011).
68. Robinson, M. D., McCarthy, D. J. & Smyth, G. K. edgeR: a Bioconductor package for differential expression analysis of digital gene expression data. *Bioinformatics* **26**, 139–140 (2010).
69. Patro, R., Duggal, G., Love, M. I., Irizarry, R. A. & Kingsford, C. Salmon provides fast and bias-aware quantification of transcript expression. *Nat. Methods* **14**, 417–419 (2017).
70. Soneson, C., Love, M. I. & Robinson, M. D. Differential analyses for RNA-seq: transcript-level estimates improve gene-level inferences. *F1000Res* **4**, 1521 (2015).
71. McCarthy, D. J., Chen, Y. & Smyth, G. K. Differential expression analysis of multifactor RNA-Seq experiments with respect to biological variation. *Nucleic Acids Res.* **40**, 4288–4297 (2012).
72. Yu, G., Wang, L. G., Han, Y. & He, Q. Y. clusterProfiler: an R package for comparing biological themes among gene clusters. *OMICS* **16**, 284–287 (2012).
73. Bouxsein, M. L. et al. Guidelines for assessment of bone microstructure in rodents using micro-computed tomography. *J. Bone Miner. Res.* **25**, 1468–1486 (2010).
74. Scheller, E. L. et al. Use of osmium tetroxide staining with microcomputerized tomography to visualize and quantify bone marrow adipose tissue in vivo. *Methods Enzymol.* **537**, 123–139 (2014).

Acknowledgements

We thank M. Handley, E. Surette and A. Galvin of the HSCI-CRM Flow Cytometry Core Facility, Massachusetts General Hospital, for assistance with cell sorting, the Center for Skeletal Research Imaging and Biomechanical Testing Core (National Institutes of Health P30 AR066261), Massachusetts General Hospital, for bone histology and µCT imaging, the Bioanalytics Core at the Diabetes and Obesity Center, Christina Lee Brown Envirome Institute, University of Louisville, for mass spectrometry analysis, the BPF Next-Gen Sequencing Core Facility at Harvard Medical School for their support for RNA-sequencing and K. Joyes for editing the manuscript. This work was funded in part by federal funds from the National Institutes of Health (HL142494, HL139598, HL131478, HL128264, AI07087, DK040561 and T32HL076136), the European Union's Horizon 2020 research and innovation program (grant agreement no. 667837), the Deutsche Forschungsgemeinschaft (CR 603/1-1, HO 5279/1-2 and RO 5071/1-1) and a fellowship from the Netherlands Organisation for Scientific Research (Rubicon Grant: 835.15.014). We acknowledge Servier Medical Art (<https://smart.servier.com>) for providing images of mice and components of the cartoon.

Author contributions

V.F., D.R. and M.N. designed experiments. V.F., D.R., G.C., N.S., M.J.S., H.A., S.C., F.F.H., F.J., I.D.v.K., F.H., L.H., C.S.M., G.S.M., S.Z., J.G., Y.I., S.P.S., G.R.W., I.-H.L. and K.G. performed experiments and collected data. V.F., D.R., G.C., N.S., F.J., I.D.v.K., G.P., S.C.A.d.J., R.I.S., I.-H.L., J.M. and K.N. analyzed data. V.F., M.J.S., D.R., S.C., F.F.H. and G.S.M. performed surgeries. V.F., D.R., G.C., N.S., H.A., P.L., G.P., P.R., D.T.S., K.N., K.L.J., F.S. and M.N. discussed results and strategy. V.F., D.R. and M.N. wrote the manuscript, which was edited by all co-authors. M.N. supervised, directed and managed the study.

Competing interests

The authors declare no competing interests.

Additional information

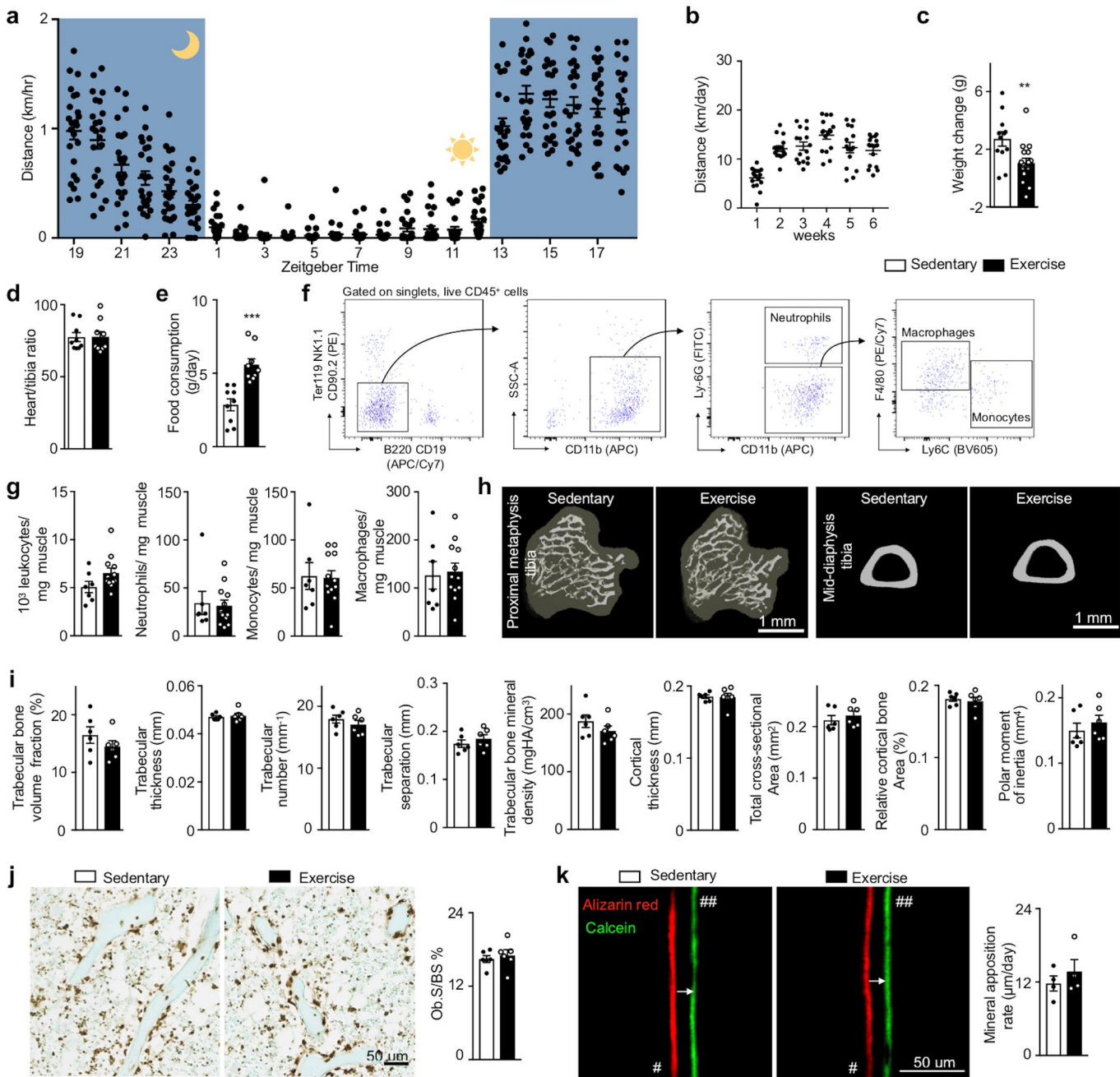
Extended data is available for this paper at <https://doi.org/10.1038/s41591-019-0633-x>.

Supplementary information is available for this paper at <https://doi.org/10.1038/s41591-019-0633-x>.

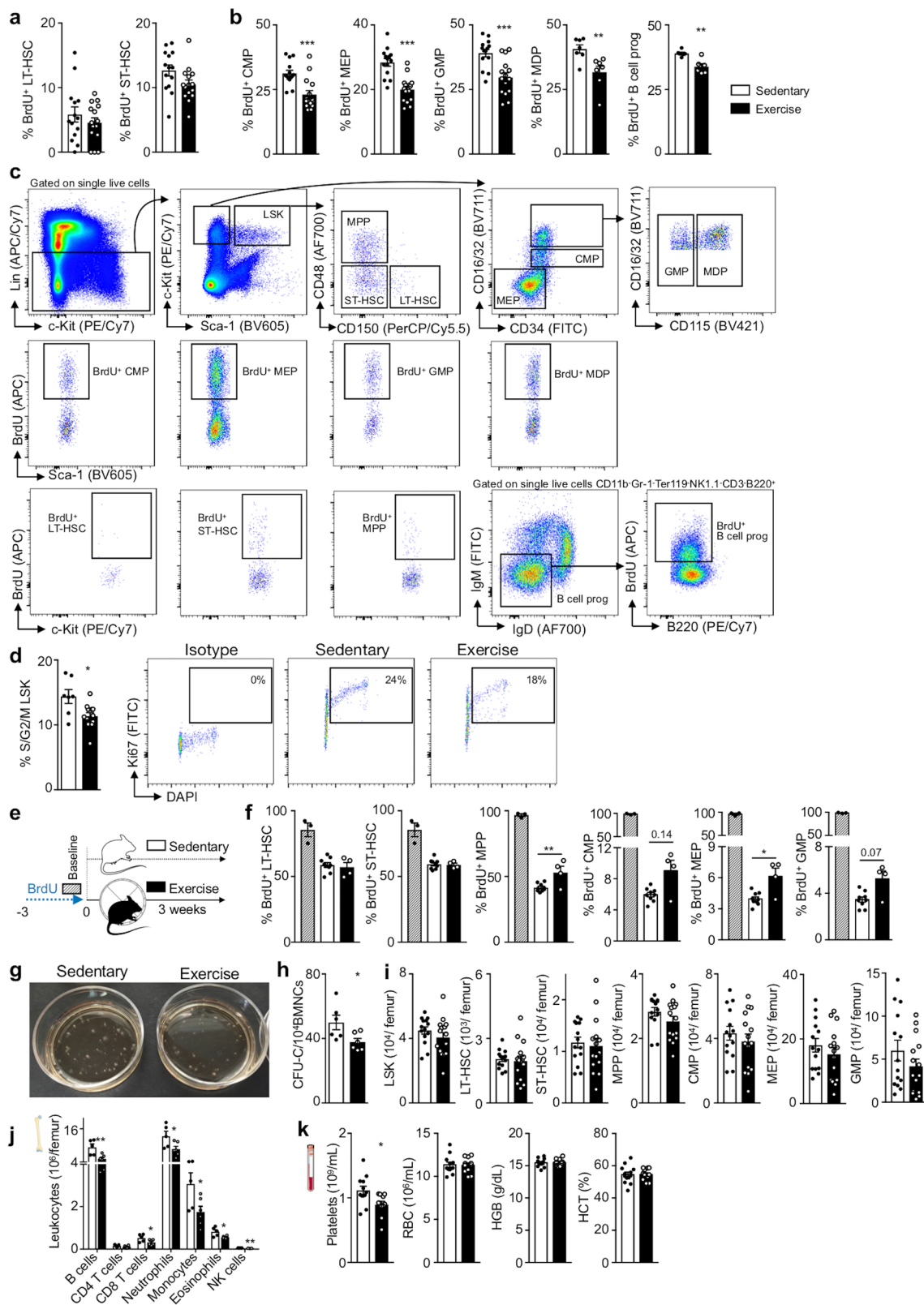
Correspondence and requests for materials should be addressed to M.N.

Peer review information Michael Basson was the primary editor on this article and managed its editorial process and peer review in collaboration with the rest of the editorial team.

Reprints and permissions information is available at www.nature.com/reprints.

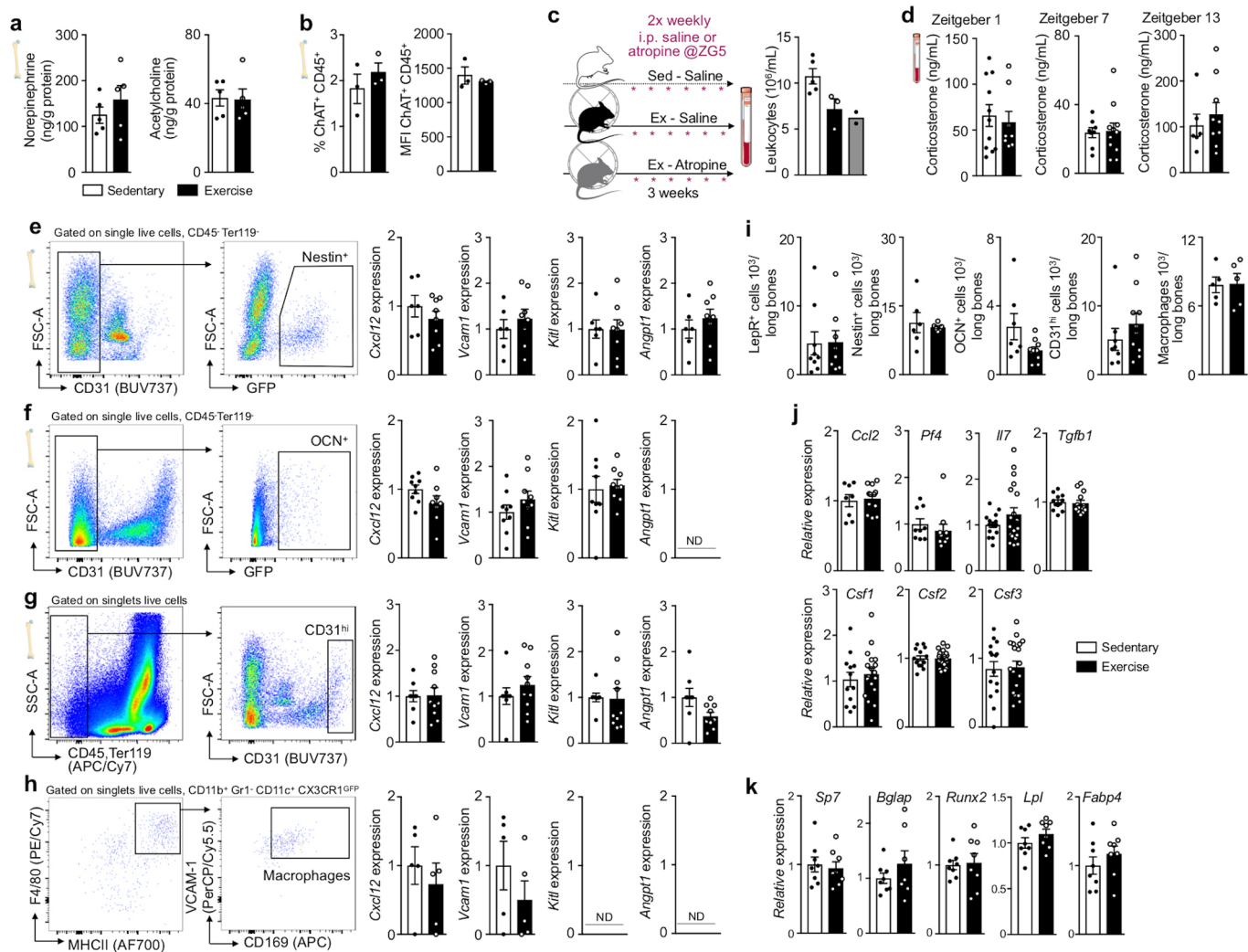


Extended Data Fig. 1 | Effects of 6 weeks of running. (a) Mean distance run per hour ($n=24$ animals). (b) Mean daily distance over the course of 6 weeks ($n=16$ animals). (c) changes in sedentary ($n=12$) and exercising mice ($n=17$, $**p=0.0076$, two-tailed U test) compared to initial six weeks prior. (d) Heart weight adjusted for tibia length ($n=9$ animals per group). (e) Food consumption during the last week of exercise ($***p=0.0002$, $n=9$ animals per group, two-tailed Student's t-test). (f) Flow cytometry gating strategy for leukocytes in skeletal muscle. (g) Total leukocytes, neutrophils, monocytes and macrophages per mg muscle tissue by flow cytometry ($n=7$ animals for sedentary, $n=12$ for exercise). (h) Representative microCT images of the proximal metaphysis and mid-diaphysis tibia of exercising and sedentary mice. (i) Parameters of bone microstructure, including trabecular and cortical thickness, bone mineral density and polar moment of inertia by μCT ($n=6$ animals per group). (j) Representative Runx2 staining of tibial proximal metaphysis. Osteoblast surface per bone surface (Ob.S/BS, $n=6$ animals per group). (k) Bone formation rate as observed by incorporation of calcein (20 mg/kg, 7 days prior) and alizarin red (30 mg/kg, 2 days prior to sacrifice) during bone mineralization at the diaphysis of femurs. Distance of fluorescent label indicated by the arrow demarcates the mineralization front at different times of administration. '#' denotes medullary cavity and '##' trabecular bone ($n=4$ animals). Data are mean \pm s.e.m. We acknowledge Servier Medical Art (<https://smart.servier.com>) for providing images of mice and components of the cartoon.

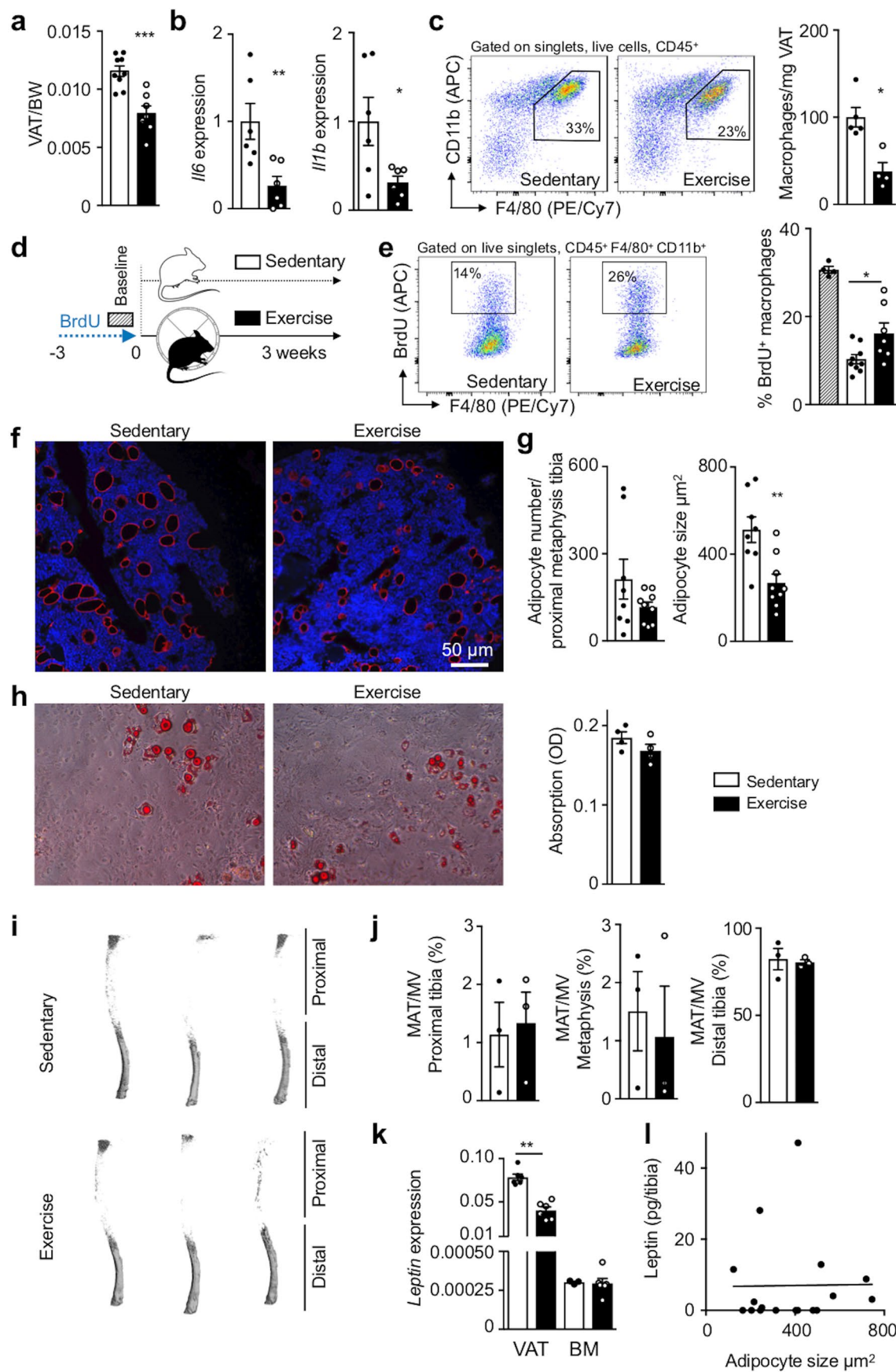


Extended Data Fig. 2 | See next page for caption.

Extended Data Fig. 2 | Increased stem and progenitor cell quiescence after 6 weeks of exercise. Mice were given 5-bromo-2- deoxyuridine (BrdU) intraperitoneally (1 mg). BrdU incorporation in (a) long-term hematopoietic stem cells (LT-HSC), short-term HSC (ST-HSC), (b) common myeloid progenitors (CMP, *** $p=0.00026$), megakaryocyte erythroid progenitors (MEP, *** $p=1.028 \times 10^{-5}$), granulocyte macrophage progenitors (GMP, *** $p=4.17 \times 10^{-4}$, all n=14 animals for sedentary, n=15 for exercise), macrophage and dendritic cell progenitors (MDP, ** $p=0.0070$, n=7 animals per group) and B cell progenitors (B cell prog, ** $p=0.0065$, n=6 animals per group) were analyzed 22 hours later (two-tailed U test for CMP, MDP and B cell prog; two-tailed Student's for MEPs and GMPs). (c) Flow cytometry gating for hematopoietic progenitors and representative flow cytometry plots of BrdU gating. (d) Cell cycle analysis in LSK assessed by Ki-67/ DAPI staining. Representative flow cytometry dot plots of + LSK (* $p=0.038$, n=7 animals for sedentary, n=12 for exercise, 2 independent experiments, two-tailed U test). (e) Experimental outline for BrdU pulse-chase experiment. Mice received BrdU in drinking water for 3 weeks (baseline, n=3 animals) prior to 3 weeks of exercise. (f) BrdU incorporation into LT-HSC, ST-HSC, multipotent progenitors (MPP, ** $p=0.0074$), CMP ($p=0.14$), MEP (* $p=0.034$) and GMP ($p=0.07$, n=9 animals for sedentary, n=4 for exercise, two-tailed U test comparing sedentary and exercise). (g) Representative images of granulocyte macrophage colonies from sedentary and running mice. (h) Bone marrow unit assay (CFU) of bone marrow mononuclear cells (BMNCs) for complete colonies (* $p=0.036$, n=6 animals per group, 2 independent experiments, two-tailed U-test). (i) Number of HSPC per femur in sedentary and exercising mice (n=15 animals per group). (j) Number of marrow leukocytes at Zeitgeber 13: B cells (** $p=0.0089$), CD4 T cells, CD8 T cells (* $p=0.048$), neutrophils (* $p=0.044$), monocytes (* $p=0.041$), eosinophils (* $p=0.019$, n=5 animals for sedentary, n=6 for exercise) and NK cells (** $p=0.00099$, n=3 per group, two-tailed U test). (k) Numbers of platelets (* $p=0.016$, two-tailed Student's), red blood cells (RBC), hemoglobin (HGB) and hematocrit (HCT, n=12 animals for sedentary and n=11 for exercise, 4 independent experiments). Data are mean \pm s.e.m. We acknowledge Servier Medical Art (<https://smart.servier.com>) for providing images of mice and components of the cartoon.

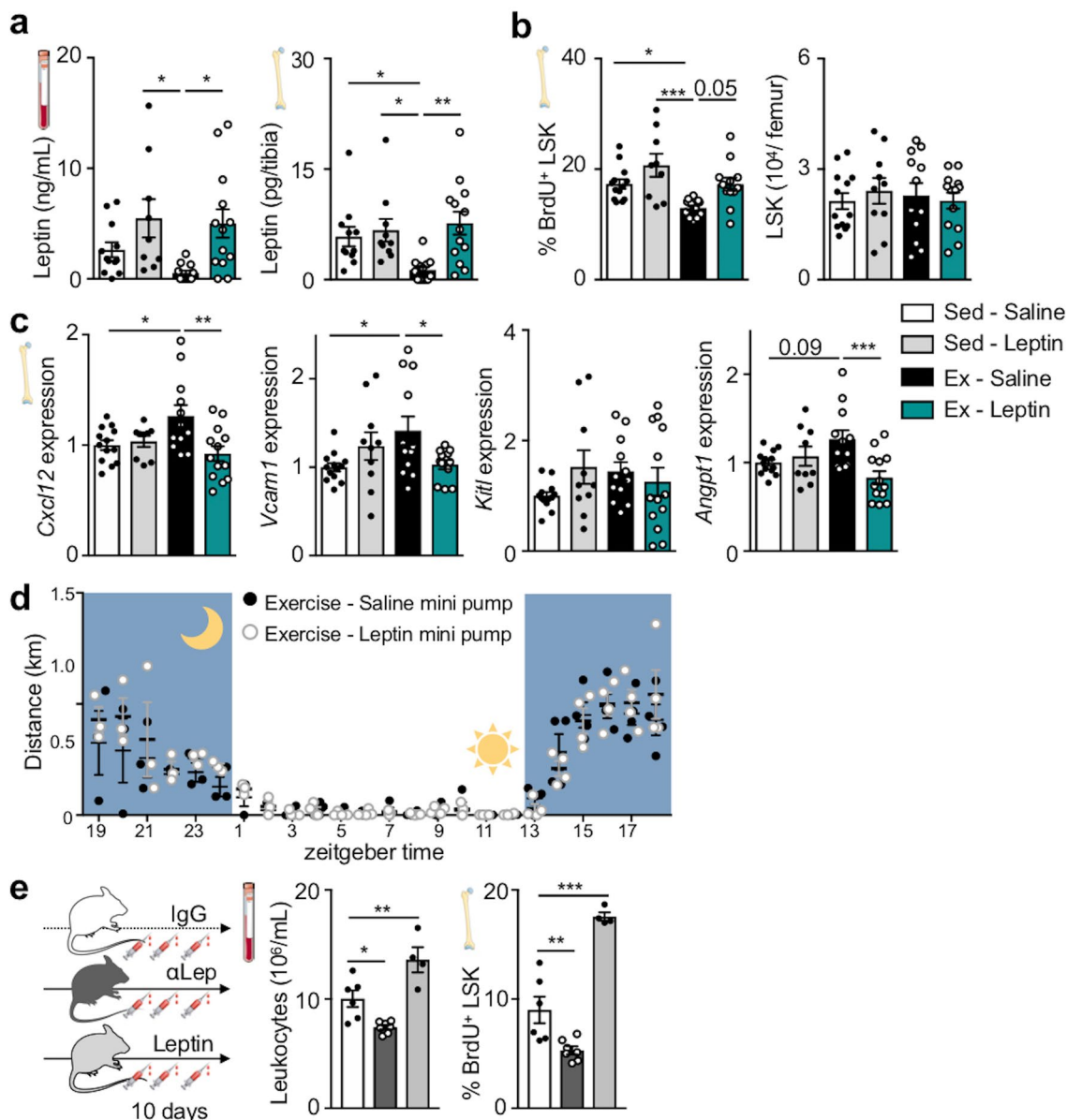


Extended Data Fig. 3 | Neutral running effects on bone marrow neurotransmitters, corticosterone and selected hematopoietic niche cells. (a) Mass spectrometry of norepinephrine and acetylcholine in the bone marrow after 6 weeks of exercise ($n=5$ animals per group). (b) Choline acetyltransferase (ChAT) expression by bone marrow CD45⁺ leukocytes ($n=3$ animals per group). (c) Experimental outline, administration of a competitive antagonist of the muscarinic acetylcholine receptors (atropine) during 3 weeks exercise. Leukocytes in circulation ($n=5$ animals for Sed-Saline, $n=3$ for Ex-Saline, $n=2$ for Ex-Atropine). (d) Plasma corticosterone at Zeitgeber time (ZG 1 ($n=11$ animals for sedentary, $n=8$ for exercise), ZG 7 ($n=8$ sedentary, $n=11$ exercise), ZG 13 ($n=6$ sedentary, $n=9$ exercise) after exercise for 6 weeks. (e) Nestin⁺ stromal cells ($n=6$ animals for sedentary, $n=8$ for exercise, 3 independent experiments), (f) OCN⁺ osteoblasts, ($n=9$ animals per group, 4 independent experiments) (g) endothelial cells ($n=8$ animals for sedentary, $n=10$ for exercise, 6 independent experiments) and (h) bone marrow macrophages ($n=5$ animals per group, 2 independent experiments) were isolated by fluorescence-activated cell sorting. GFP stromal reporter mice either had access to exercise wheels for 6 weeks or remained sedentary. Representative dot plots are shown. Expression of Cxcl12, Vcam1, Kitl and Angpt1 was assessed by qPCR, ND: not detectable. (i) Numbers of stromal niche cells in sedentary and exercising mice ($n=9$ and $n=8$ for LepR⁺, $n=6$ and $n=8$ for Nestin⁺, $n=9$ and $n=9$ for OCN⁺, $n=8$ and $n=10$ for CD31^{hi}, $n=5$ and $n=5$ animals for sedentary and exercise, respectively). (j) Gene expression of several niche factors in total bone marrow by qPCR ($n=8$ animals for sedentary for Ccl2 and Pf4, $n=12$ for sedentary for Tgfb, Csf1, $n=16$ for sedentary for Il7, Csf2, Csf3, $n=13$ for exercise for Ccl2, Tgfb, $n=19$ for exercise for Il7, Csf1, Csf2, Csf3, 4 independent experiments). (k) Markers for osteolineage cells (Sp7, Bglap, Runx2) and adipocytes (Lpl, Fabp4) by qPCR in total bone marrow ($n=8$ animals per group, 2 independent experiments). All mRNA levels were normalized to Actb Ct values. Data are mean \pm s.e.m., where appropriate. We acknowledge Servier Medical Art (<https://smart.servier.com>) for providing images of mice and components of the cartoon.

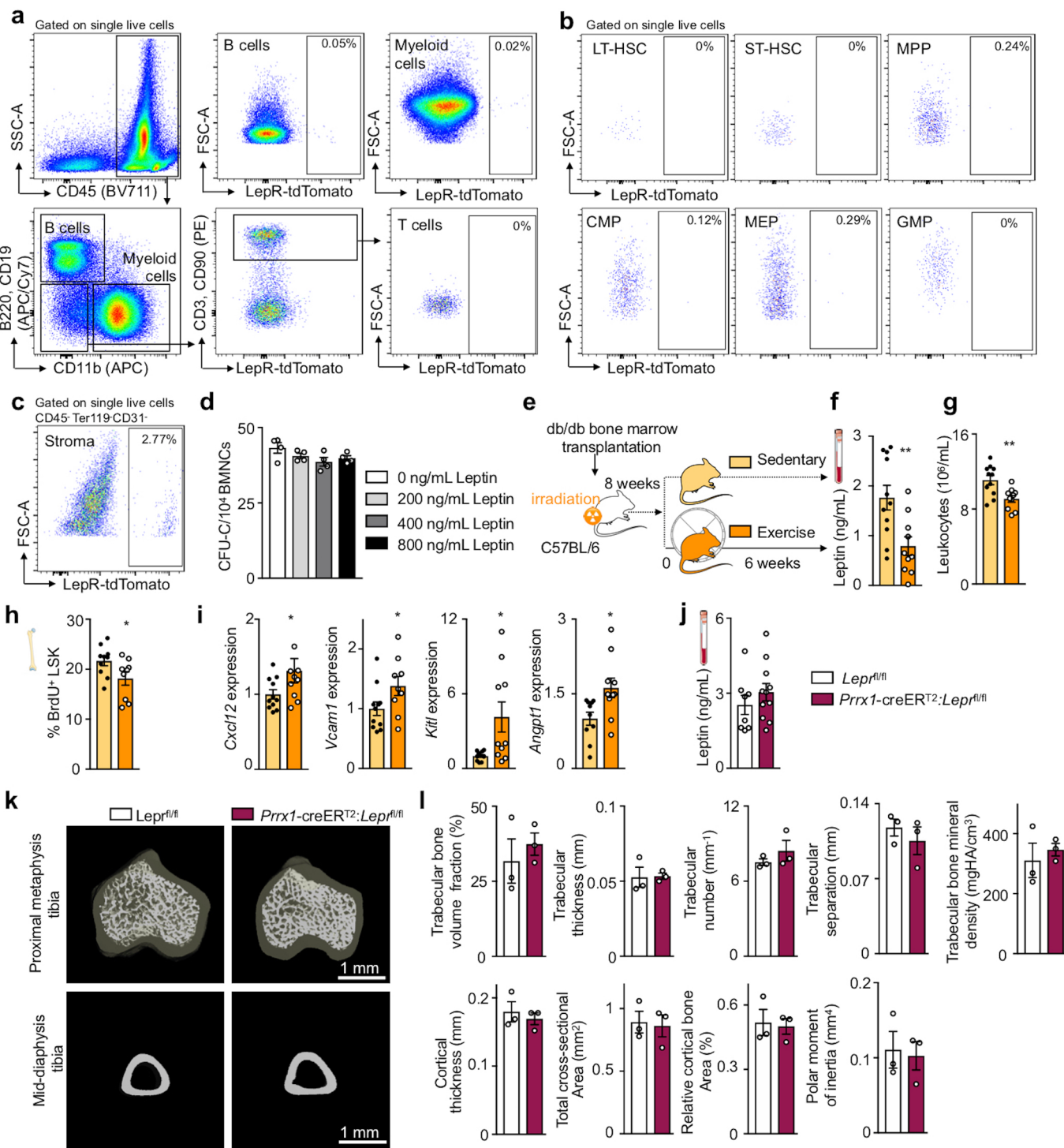


Extended Data Fig. 4 | See next page for caption.

Extended Data Fig. 4 | Exercise reduces visceral adipose tissue macrophages. (a) Visceral adipose tissue (VAT) per mouse adjusted for (BW; *** $p=0.00069$, n=9 animals for sedentary, n=7 for exercise, 2 independent experiments, two-tailed U test). (b) Cytokine production by visceral adipose tissue by qPCR (* $p=0.034$, ** $p=0.0087$, n=6 animals per group, 2 independent experiments, two-tailed U test). (c) Macrophages per mg VAT. Representative dot plots are shown (* $p=0.016$, n=5 animals for sedentary, n=4 for exercise, two-tailed U test). (d) Experimental outline for e. Mice received BrdU in drinking water for 3 weeks (baseline, n=4 animals) prior to 3 weeks of exercise. (e) BrdU incorporation into VAT macrophages (* $p=0.045$, n=9 animals for sedentary, n=7 for exercise, 2 independent experiments, two-tailed U test comparing sedentary and exercise). Representative dot plots are shown. (f) Longitudinal sections of tibias were stained by perilipin (red) and counterstained by DAPI (blue). (g) Quantification of adipocyte numbers and size in the proximal metaphysis of tibias (** $p=0.0055$, n=8 animals for sedentary, n=9 for exercise, 3 independent experiments, two-tailed U -test). (h) In vitro adipocyte differentiation assay of bone marrow stromal cells from all long bones and pelvic bones. Representative images with 100x magnification are shown (n=4 animals per group). (i,j) Visualization of marrow adipose tissue in tibias by osmium stain by μ CT and marrow adipose tissue (MAT) per marrow volume (MV) (n=3 animals per group). (k) Leptin expression by qPCR in visceral adipose tissue (VAT; ** $p=0.0022$, n=6 animals per group, two-tailed U test) and bone marrow (BM; n=3 animals for sedentary, n=6 for exercise). mRNA levels were normalized to *Actb* Ct values. Data are mean \pm s.e.m. (l) Lack of correlation between tibial adipocyte size and leptin concentration ($R^2=0.0002$, P=0.96, n=17 animals, linear regression analysis). We acknowledge Servier Medical Art (<https://smart.servier.com>) for providing images of mice and components of the cartoon.

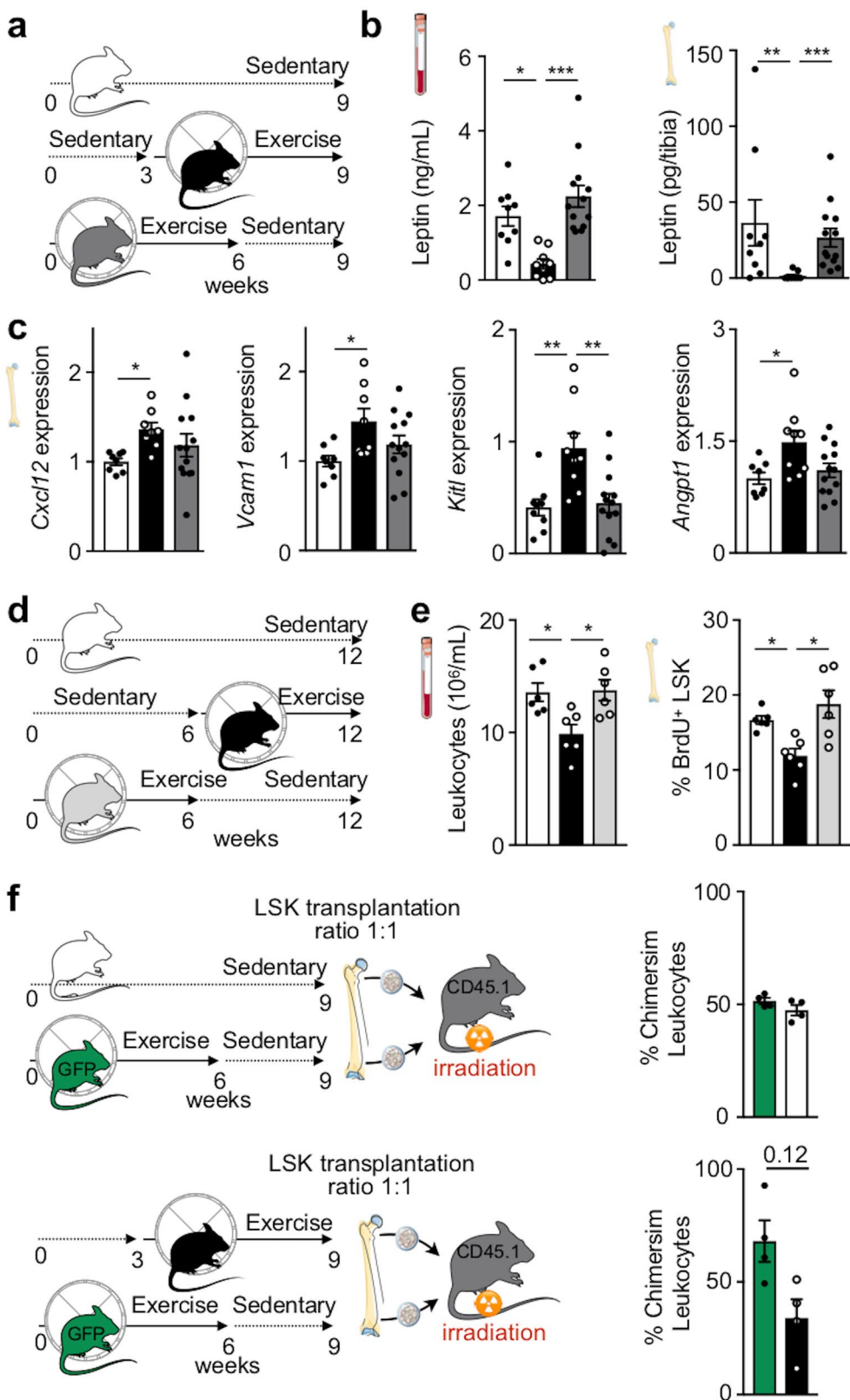


Extended Data Fig. 5 | Leptin supplementation and antibody neutralization. **(a)** Leptin levels in blood (* $p=0.19$ for both sed-leptin vs ex-saline and ex-saline vs ex-leptin, one-way analysis of variance with Sidak's post hoc test) and bone marrow (* $p=0.013$ sed-leptin vs ex-saline, * $p=0.042$ sed-saline vs ex-saline, ** $p=0.0038$ ex-saline versus ex-leptin, $n=12$ animals for sed-saline and ex-saline, $n=10$ for sed-leptin, $n=13$ for ex-leptin, 5 independent experiments, with Dunn's post hoc test) as measured by ELISA. **(b)** LSK proliferation 22 h after intraperitoneal injection of BrdU (* $p=0.047$ sed-saline versus ex-sal, $P=0.05$ ex-saline versus ex-leptin, ** $p=0.00031$ sed-leptin versus ex-sal, $n=12$ animals for sed-saline and ex-saline, $n=10$ for sed-leptin, $n=13$ for ex-leptin, 5 independent experiments, one-way analysis of variance with Sidak's post hoc test), LSK numbers and **(c)** expression of hematopoietic factors in bone marrow of exercising and sedentary mice implanted with osmotic minipumps as described in Fig. 2h (* $p=0.016$ and ** $p=0.0026$ for Cxcl12, * $p=0.025$ sed-saline versus ex-saline and * $p=0.046$ ex-saline versus ex-leptin for Vcam1, *** $p=0.00074$ ex-saline versus ex-leptin and $p=0.09$ sed-saline versus ex-saline for Angpt1, $n=12$ animals for sed-saline and ex-saline, $n=10$ for sed-leptin, $n=13$ for Ex-Leptin). **(d)** Running distance with either saline or leptin and access to exercise wheels for 6 weeks. Mean distance run per hour ($n=4$ animals per group). **(e)** Injection of antibody or leptin into sedentary mice. Circulating leukocytes levels at Zeitgeber time 7 (* $p=0.010$ IgG versus αLep, ** $p=0.0072$ αLep versus leptin) and LSK proliferation 22 h after intraperitoneal injection (** $p=0.0038$ IgG versus αLep, *** $p=1.52 \times 10^{-5}$, $n=6$ animals for IgG, $n=7$ for αLep, $n=4$ for Leptin, 2 independent experiments, one-way analysis of variance with Sidak's post hoc test). Data are mean \pm s.e.m. We acknowledge Servier Medical Art (<https://smart.servier.com>) for providing images of mice and components of the cartoon.



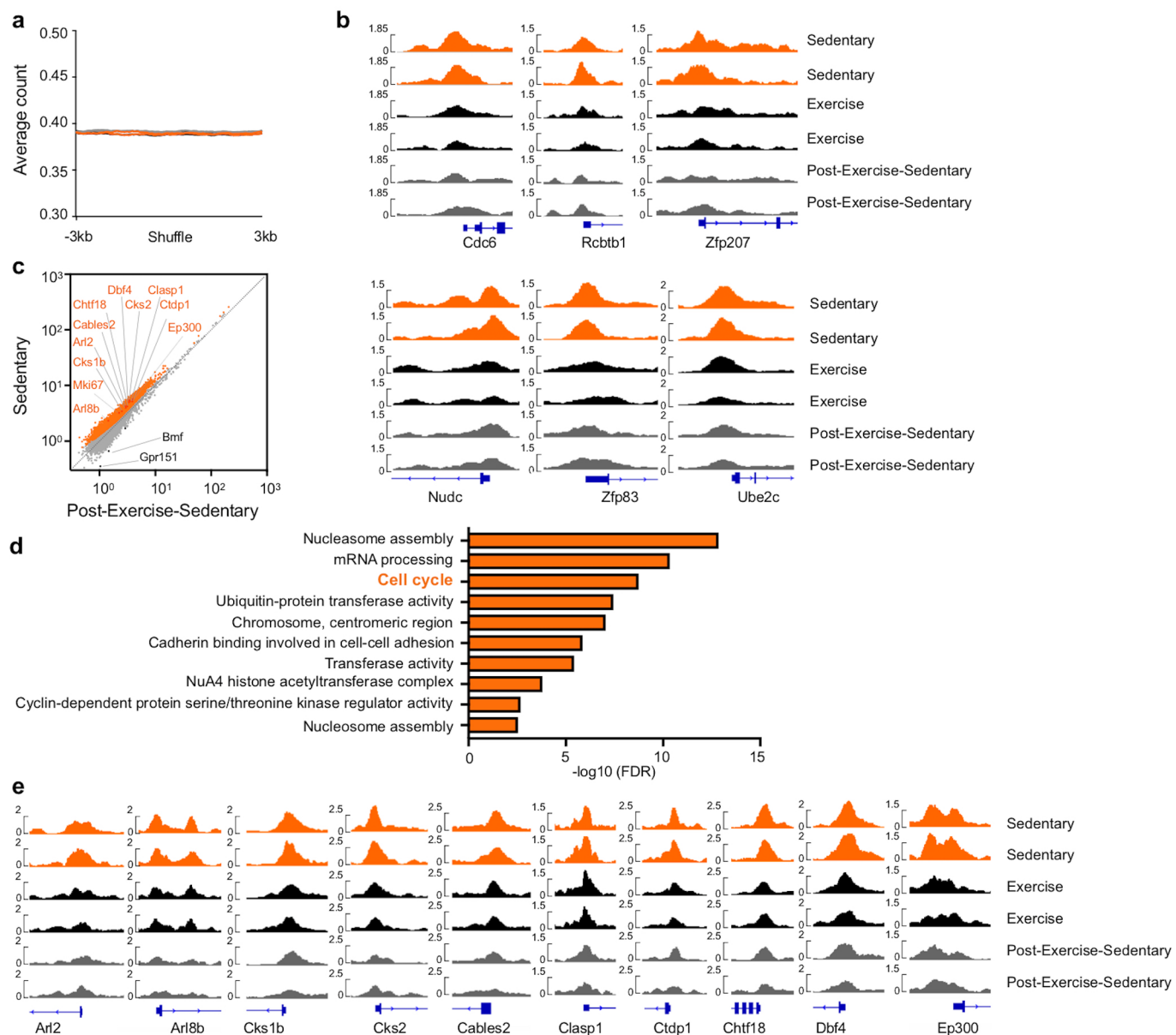
Extended Data Fig. 6 | See next page for caption.

Extended Data Fig. 6 | Leptin receptor expression in the bone marrow. (a) Representative flow cytometry dot plots of leptin receptor (LepR) expression in B cells, myeloid cells, T cells, (b) bone marrow long-term hematopoietic stem cells (LT-HSC), short-term HSC (ST-HSC), multipotent progenitors (MPP), common myeloid progenitors (CMP), megakaryocyte erythroid progenitors (MEP), granulocyte macrophage progenitors (GMP) and (c) stromal bone marrow cells ($n=3$ independent experiments with similar results). (d) Bone marrow unit assay (CFU) for complete colonies ($n=4$ donor animals). Bone marrow mononuclear cells (BMNCs) were plated with increasing concentrations of leptin. (e) Experimental outline for bone marrow transplantation; data shown in panel f-i. Total bone marrow was isolated from db/db donor mice and transplanted into wild type recipients. After an 8-week recovery period, mice exercised for 6 weeks or remained sedentary. (f) Leptin levels in serum by ELISA ($**p=0.0059$, $n=11$ animals for sedentary, $n=10$ for exercise, 2 independent experiments, two-tailed Student's t-test). (g) Circulating leukocyte levels at Zeitgeber time 7 ($**p=0.0042$, $n=11$ for animals sedentary, $n=10$ for exercise, 2 independent experiments, two-tailed Student's t-test). (h) BrdU incorporation into LSK 22 h after intraperitoneal injection ($*p=0.045$, $n=10$ animals sedentary, $n=9$ for exercise, 2 independent experiments, two-tailed Student's t-test). (i) Gene expression by qPCR in total bone marrow of *Cxcl12* ($*p=0.042$), *Vcam1* ($*p=0.03$), *Kitl* ($*p=0.014$) and *Angpt1* ($*p=0.0168$, $n=11$ animals for sedentary, $n=10$ for exercise, 2 independent experiments, two-tailed U test for *Cxcl12* and two-tailed Student's t-test for *Vcam1*, *Kitl*, *Angpt1*). mRNA levels were normalized to *Actb* Ct values. (j) Leptin levels in blood of *Lep^{dfl/fl}* and *Prxx1-creERT²:Lep^{dfl/fl}* mice measured by ELISA ($n=8$ animals for *Lep^{dfl/fl}* and $n=11$ for *Prxx1-creERT²:Lep^{dfl/fl}*). (k) Representative microCT images of the proximal metaphysis and mid-diaphysis tibia of *Prxx1-creERT²:Lep^{dfl/fl}* mice and their *Lep^{dfl/fl}* littermates. (l) Parameters of bone microstructure, including trabecular and cortical thickness, bone mineral density and polar moment of inertia by μCT ($n=3$ animals per group). Data are mean \pm s.e.m. We acknowledge Servier Medical Art (<https://smart.servier.com>) for providing images of mice and components of the cartoon.

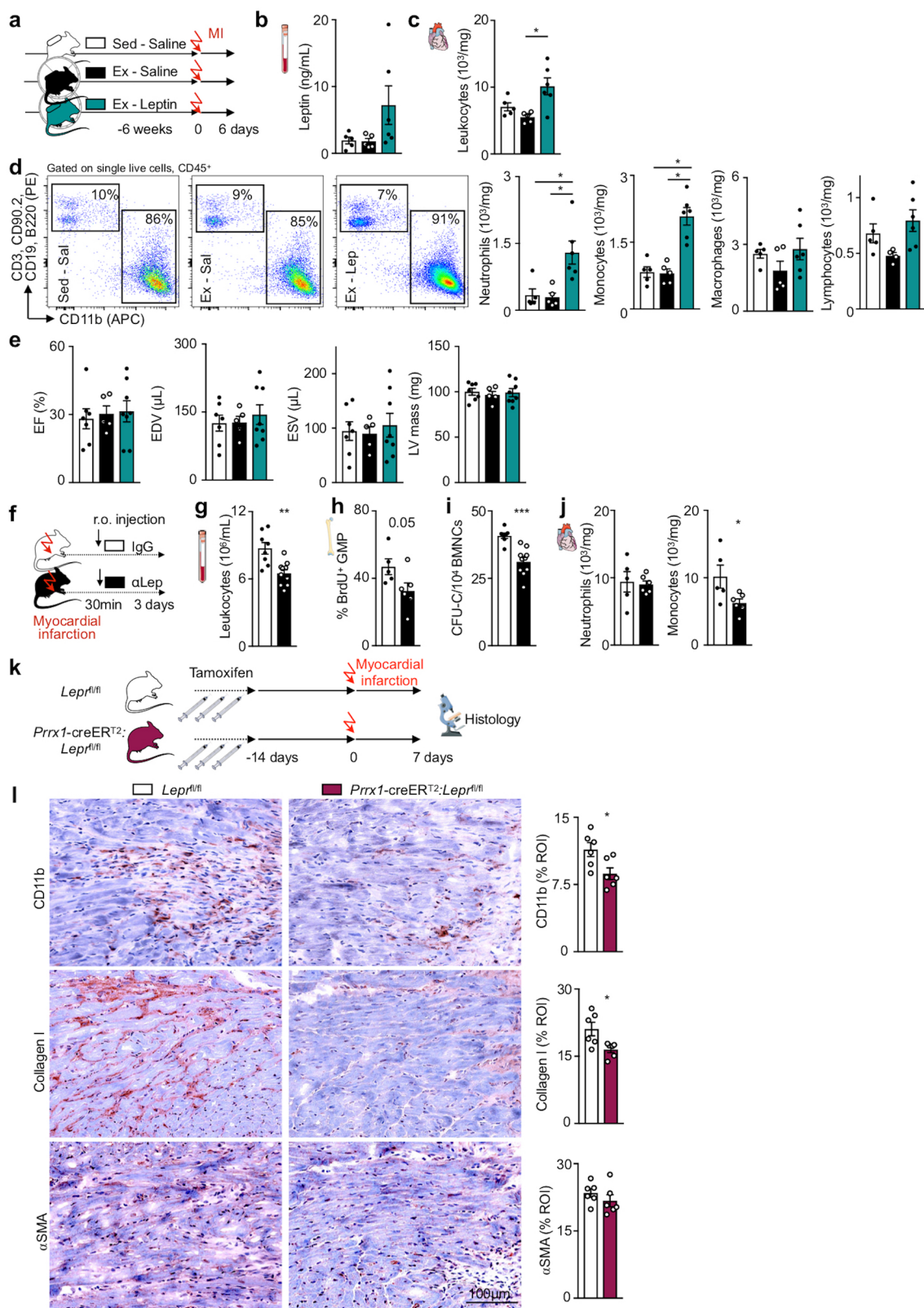


Extended Data Fig. 7 | See next page for caption.

Extended Data Fig. 7 | Exercise effects wane after 6 sedentary weeks. (a) Experimental outline for b-c. (b) Blood (* $p=0.012$, *** $p=8.89\times10^{-5}$) and tibial (** $p=0.0053$, *** $p=0.00079$) leptin concentrations measured by ELISA ($n=9$ animals for sedentary and exercise, $n=13$ animals for post-exercise-sedentary, 3 independent experiments, with Dunn's post hoc test). (c) Gene expression of niche factors *Cxcl12* (* $p=0.015$), *Vcam1* (* $p=0.038$), *Kitl* (** $p=0.0037$ sedentary versus exercise, ** $p=0.0035$ exercise versus post-exercise-sedentary) and *Angpt1* (* $p=0.027$) in whole bone marrow by qPCR ($n=9$ animals for sedentary and exercise, $n=13$ animals for post-exercise-sedentary, 3 independent experiments, one-way analysis of variance with Sidak's post hoc test). mRNA levels were normalized to *Actb* Ct values. (d) Experimental outline for e. The post-exercise-sedentary group had access to exercise wheels for 6 weeks after which the wheels were removed for the following 6 weeks. Sedentary controls had no access, while the exercise group had access to wheels during the last 6 weeks before sacrifice. (e) Circulating leukocyte levels at Zeitgeber time 7 (* $p=0.028$ sedentary versus exercise, * $p=0.045$ exercise versus post-exercise sedentary) and BrdU incorporation into LSK 22 h after intraperitoneal injection (* $p=0.045$ sedentary versus exercise, * $p=0.014$ exercise versus post-exercise-sedentary, $n=6$ animals per group, with Dunn's post hoc test). (f) Outline of the competitive bone marrow transplantation experiments. LSK were isolated from CD45.2 donors that either exercised for 6 weeks or were sedentary. These were transplanted in a 1:1 ratio into CD45.1 recipients together with LSK isolated from Ubc-GFP mice that exercised for 6 weeks and had a 3-week post-exercise-sedentary period. Blood chimerism 8 weeks after transplantation ($n=4$ animals per group, $p=0.12$ for exercise versus post-exercise-sedentary donor chimerism, Wilcoxon matched-pairs signed rank test). Data are mean \pm s.e.m. We acknowledge Servier Medical Art (<https://smart.servier.com>) for providing images of mice and components of the cartoon.

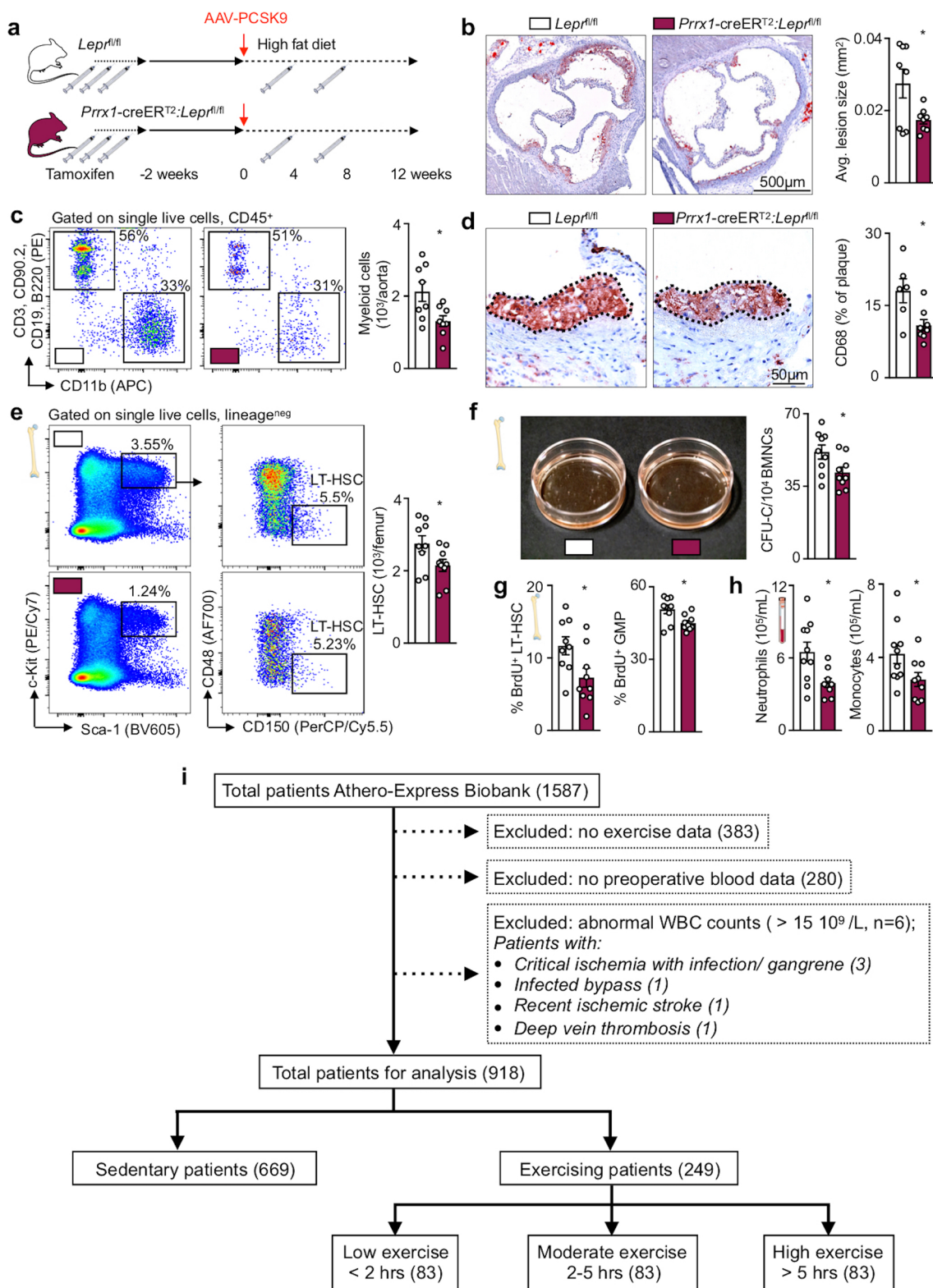


Extended Data Fig. 8 | Background ATAC-seq signals are similar, while peaks are higher in LSK of sedentary mice. (a) Average profiles of ATAC-seq tag density among randomly shuffled regions of the same size as the actual ATAC-seq peaks. These profiles are similar among different conditions, suggesting the absence of background shift between ATAC-seq signals. (b) Tracks of normalized ATAC-seq tag density for the loci of additional genes in the top ten significant genes in the cell cycle category as determined by DAVID in Fig. 3n. (c) Scatter plot of normalized tag density at ATAC-seq peaks shows comparison between LSK from sedentary versus post-exercise-sedentary cohorts. Peaks with significantly lower and higher tag density in post-running mice are highlighted in orange and black, respectively ($FDR < 0.01$). The top ten significant genes in the cell cycle pathway determined by DAVID (refer to d) and *Mki67* are indicated; see Supplementary Table 1 for all genes. (d) Functional categories enriched among genes with differential chromatin accessibility in LSK from sedentary versus post-exercise-sedentary mice as determined by DAVID. (e) Tracks of normalized ATAC-seq tag density for the loci of the top ten significant genes in the cell cycle category as determined by DAVID in d.



Extended Data Fig. 9 | See next page for caption.

Extended Data Fig. 9 | Leptin in acute MI. (a) Experimental outline for b-e. (b) Leptin blood levels on day 6 after MI ($n=5$ animals for Sed-Saline and Ex-Saline, $n=6$ for Ex-Leptin, 3 independent experiments). (c) Infarct CD45⁺ leukocyte levels on day 6 after MI (* $p=0.025$, $n=5$ animals for Sed-Saline and Ex-Saline, $n=6$ for Ex-Leptin, 3 independent experiments, with Dunn's post hoc test). (d) Flow cytometry gating and quantification of neutrophils (* $p=0.039$ Sed-Saline versus Ex-Leptin, * $p=0.021$ Ex-Saline versus Ex-Leptin), monocytes (* $p=0.018$ Sed-Saline versus Ex-Leptin, * $p=0.015$ Ex-Saline versus Ex-Leptin), macrophages and lymphocytes in the infarct in respective cohorts ($n=5$ animals for Sed-Saline and Ex-Saline, $n=6$ for Ex-Leptin, 3 independent experiments, with Dunn's post hoc test). (e) Cardiac magnetic resonance imaging on day 21 after MI. Ejection fraction (EF), enddiastolic volume (EDV), endsystolic volume (ESV) and left ventricular (LV) mass were determined ($n=7$ animals for Sed-Saline, $n=5$ for Ex-Saline, $n=8$ for Ex-Leptin, 3 independent experiments). (f) Experimental outline for panels g-j. (g) Circulating leukocytes at Zeitgeber 7 (** $p=0.0017$, $n=8$ animals for IgG and $n=10$ for α Lep, 3 independent experiments, two-tailed Student's). (h) BrdU incorporation into granulocyte macrophage progenitors (GMP) 3 days after MI ($p=0.05$, $n=8$ animals for IgG and $n=10$ for α Lep, 3 independent experiments, two-tailed Student's t-test). (i) Bone marrow unit assay (CFU) of bone marrow mononuclear cells (BMNCs) for complete colonies (** $p=0.00041$, $n=7$ animals for IgG and $n=10$ for α Lep, 3 independent experiments, two-tailed U test). (j) Neutrophils and monocytes per mg infarct tissue (* $p=0.03$, $n=5$ animals for IgG, $n=6$ for α Lep, two-tailed U test). (k) Experimental outline for l. (l) Representative immunohistochemical stainings and quantification of myeloid cells (CD11b), collagen deposition (Collagen I), and myofibroblasts (alpha smooth muscle actin) in the infarct border zone (* $p=0.026$ for CD11b and Collagen I, $n=6$ animals per group, two-tailed U test). Data are mean \pm s.e.m. We acknowledge Servier Medical Art (<https://smart.servier.com>) for providing images of mice and components of the cartoon.



Extended Data Fig. 10 | See next page for caption.

Extended Data Fig. 10 | Stromal leptin receptor deletion attenuates atherosclerosis, inflammation and hematopoiesis. (a) Experimental outline for b-h. *Lep^{r/r}* mice and *Prrx1-creER^{T2}:Lep^{r/r}* littermates were injected with tamoxifen and received a single IV injection of AAV-PCSK9 followed by a high fat diet for 12 weeks. (b) Representative cross sections of aortic roots stained with Oil red O and assessment of lesion size (*p=0.042, n=8 animals per group, two-tailed Student's t-test). (c) Flow cytometry enumeration of myeloid cells in aortas of *Lep^{r/r}* and *Prrx1-creER^{T2}:Lep^{r/r}* mice (*p=0.023, n=8 animals per group, two-tailed Student's t-test). (d) CD68 histological staining of aortic root lesions. Percentage of positive staining per plaque (*p=0.029, n=6 animals for *Lep^{r/r}*, n=8 for *Prrx1-creER^{T2}:Lep^{r/r}*, two-tailed U test). (e) Representative flow plots and statistical analysis of long-term hematopoietic stem cells (LT-HSC) in femur bone marrow (*p=0.046, n=9 animals per group, two-tailed Student's t-test). (f) Bone marrow unit assay for complete colonies (CFU-C) of bone marrow mononuclear cells (BMNCs) (*p=0.036, n=9 animals per group, two-tailed Student's t-test). (g) BrdU incorporation assay 22 hours after intraperitoneal injection for LT-HSC and progenitors (GMP) proliferation (*p=0.027 for LT-HSC, *p=0.017 for GMP, n=9 animals per group, two-tailed Student's t-test). (h) Circulating myeloid cells at Zeitgeber time 7 (*p=0.014 for neutrophils, *p=0.046 for monocytes, n=10 animals for *Lep^{r/r}*, n=9 for *Prrx1-creER^{T2}:Lep^{r/r}*, two-tailed Student's t-test). Data are mean±s.e.m. (i) Athero-express cohort. The illustrates inclusion criteria for patients and separation into sedentary lifestyle and exercise groups. We acknowledge Servier Medical Art (<https://smart.servier.com>) for providing images of mice and components of the cartoon.

Reporting Summary

Nature Research wishes to improve the reproducibility of the work that we publish. This form provides structure for consistency and transparency in reporting. For further information on Nature Research policies, see [Authors & Referees](#) and the [Editorial Policy Checklist](#).

Statistics

For all statistical analyses, confirm that the following items are present in the figure legend, table legend, main text, or Methods section.

n/a Confirmed

- The exact sample size (n) for each experimental group/condition, given as a discrete number and unit of measurement
- A statement on whether measurements were taken from distinct samples or whether the same sample was measured repeatedly
- The statistical test(s) used AND whether they are one- or two-sided
Only common tests should be described solely by name; describe more complex techniques in the Methods section.
- A description of all covariates tested
- A description of any assumptions or corrections, such as tests of normality and adjustment for multiple comparisons
- A full description of the statistical parameters including central tendency (e.g. means) or other basic estimates (e.g. regression coefficient) AND variation (e.g. standard deviation) or associated estimates of uncertainty (e.g. confidence intervals)
- For null hypothesis testing, the test statistic (e.g. F , t , r) with confidence intervals, effect sizes, degrees of freedom and P value noted
Give P values as exact values whenever suitable.
- For Bayesian analysis, information on the choice of priors and Markov chain Monte Carlo settings
- For hierarchical and complex designs, identification of the appropriate level for tests and full reporting of outcomes
- Estimates of effect sizes (e.g. Cohen's d , Pearson's r), indicating how they were calculated

Our web collection on [statistics for biologists](#) contains articles on many of the points above.

Software and code

Policy information about [availability of computer code](#)

Data collection

All flow cytometry data were acquired on an LSRII or FACSaria II (BD Biosciences) using FACSDiva v8.0.3 software. ATAC-seq DNA libraries were sequenced on an Illumina HiSeq 2500. RNA-seq DNA libraries were sequenced on an Illumina NextSeq 500. qPCR data were acquired on an Applied Biosystems 7500 Fast Real-Time PCR System. Histology slides were scanned with a NanoZoomer 2.0RS (Hamamatsu).

Data analysis

Flow Cytometry data were analyzed with FlowJo 10.3.0 software. Cardiac MRI data were analyzed with HOROS software. ATAC-seq data were analyzed using BWA-MEM, HOTSPOT2 and edgeR software. RNA-seq data were analyzed using Salmon, tximport, edgeR and clusterProfiler. ImageJ 1.51a was used for histology image analysis. SPSS 21.0 and GraphPad Prism 7.0c were used for statistical analysis.

For manuscripts utilizing custom algorithms or software that are central to the research but not yet described in published literature, software must be made available to editors/reviewers. We strongly encourage code deposition in a community repository (e.g. GitHub). See the Nature Research [guidelines for submitting code & software](#) for further information.

Data

Policy information about [availability of data](#)

All manuscripts must include a [data availability statement](#). This statement should provide the following information, where applicable:

- Accession codes, unique identifiers, or web links for publicly available datasets
- A list of figures that have associated raw data
- A description of any restrictions on data availability

Raw sequencing data are available from Gene Expression Omnibus, accession numbers GSE110639 and GSE124799.

Field-specific reporting

Please select the one below that is the best fit for your research. If you are not sure, read the appropriate sections before making your selection.

- Life sciences Behavioural & social sciences Ecological, evolutionary & environmental sciences

For a reference copy of the document with all sections, see nature.com/documents/nr-reporting-summary-flat.pdf

Life sciences study design

All studies must disclose on these points even when the disclosure is negative.

Sample size	No statistical methods were used to predetermine sample size. We did all experiments at least 2-3 times, with groups of at least n=3-5. From previous experience on either HSPC biology, niche factors, and inflammatory responses, we estimated how many mice we would approximately need.
Data exclusions	Statistical outliers (not more than one per experiment) were determined with the two-sided Grubbs' outlier test (GraphPad Prism) and excluded.
Replication	All experiments were reproduced at least once. All reproductions were successful.
Randomization	Mice were randomly assigned to groups at the start of experiments. For ApoE-/ mice, we determined leukocyte counts in all mice after 10 weeks of diet and allocated them into two groups of equal leukocyte counts to ensure same starting leukocyte levels prior to determining effects of exercise.
Blinding	Investigators were generally not blinded to group allocation. However, the analysis of the effect of exercise prior to cecal ligation and puncture as well as myocardial infarction and the effect of leptin inhibition after myocardial infarction were performed in a blinded fashion.

Reporting for specific materials, systems and methods

We require information from authors about some types of materials, experimental systems and methods used in many studies. Here, indicate whether each material, system or method listed is relevant to your study. If you are not sure if a list item applies to your research, read the appropriate section before selecting a response.

Materials & experimental systems		Methods	
n/a	Involved in the study	n/a	Involved in the study
<input type="checkbox"/>	<input checked="" type="checkbox"/> Antibodies	<input checked="" type="checkbox"/>	ChIP-seq
<input checked="" type="checkbox"/>	<input type="checkbox"/> Eukaryotic cell lines	<input type="checkbox"/>	<input checked="" type="checkbox"/> Flow cytometry
<input checked="" type="checkbox"/>	<input type="checkbox"/> Palaeontology	<input checked="" type="checkbox"/>	<input type="checkbox"/> MRI-based neuroimaging
<input type="checkbox"/>	<input checked="" type="checkbox"/> Animals and other organisms		
<input type="checkbox"/>	<input checked="" type="checkbox"/> Human research participants		
<input checked="" type="checkbox"/>	<input type="checkbox"/> Clinical data		

Antibodies

Antibodies used

Antibodies used for flow cytometry (all purchased from BioLegend unless indicated otherwise):
 Biotin-conjugated antibodies (dilution for all 1:300): CD3 (100304, clone 145-2C11), CD4 (100404, clone GK1.5), CD8α (100704, clone 53-6.7), CD49b (108904, clone DX5), CD90.2 (105304, clone 30-H12), CD19 (115503, clone 6D5), B220 (103204, clone RA3-6B2), NK1.1 (108704, clone PK136), TER119 (116204, clone TER-119), CD11b (101204, clone M1/70), CD11c (117304, clone N418), Gr1 (108404, clone RB6-8C5).
 PE-conjugated antibodies (dilution for all 1:300): B220 (103208, clone RA3-6B2), CD19 (115508, clone 6D5), CD3 (100206, clone 17A2), CD90.2 (140308, clone 53-2.1), CD49b (108908, clone DX5), CD103 (121406, clone 2E7), NK1.1 (108708, PK136) and Ter119 (116208, clone TER-119).
 Antibodies conjugated to other fluorophores (dilution 1:300 unless stated otherwise): CD16/32-BV711 (101337, clone 93, 1:150), CD34-FITC (553733, clone RAM34, BD Biosciences, 1:150), CD48-AF700 (103426, clone HM48-1), CD115-BV421 (135513, clone AFS98), CD150-PerCP/Cy5.5 (115922, clone TC15-12F12.2), c-kit-PE/Cy7 (105814, clone 2B8, 1:150), Sca-1-BV605 (108133, clone D7, 1:150), BrdU-APC (552598, BD Biosciences, 1:50), Ki-67-FITC (11-5698-82, Thermo Fisher Scientific), CD11b-APC (101212, clone M1/70), CD45-BV711 (103147, clone 30-F11), F4/80-PECy7 (123114, clone BM8), Ly-6C-BV605 (128035, clone HK1.4), Ly-6G-FITC (127605, clone 1A8), B220-PE/Cy7 (103222, clone RA3-6B2), B220-APC/Cy7 (103224, clone RA3-6B2), CD3-PE (100206, clone 17A2), CD4-PerCP/Cy5.5 (100434, clone GK1.5), CD8α-BV711 (100748, clone 53-6.7), CD19-PE/Cy7 (115520, clone 6D5), CD19-APC/Cy7 (115530, clone 6D5), CD45.2-AF700 (109822, clone 104), NK1.1-APC/Cy7 (108730, clone PK136).

Antibodies used for in vivo experiments:

Mouse Leptin/OB Antibody (AF498, R&D Systems) and Normal Goat IgG Control (AB-108-C, R&D Systems).

Validation

All antibodies used for flow cytometry were previously validated for flow cytometry on murine cells by the respective manufacturers.

In vitro and in vivo validation of the anti-leptin antibody was previously performed by Konstantinides et al. (Konstantinides S, Schäfer K, Neels JG, Dellas C, Loskutoff DJ. Inhibition of endogenous leptin protects mice from arterial and venous thrombosis. *Arterioscler Thromb Vasc Biol* 2004; 24(11): 2196-2201).

Animals and other organisms

Policy information about [studies involving animals; ARRIVE guidelines](#) recommended for reporting animal research

Laboratory animals

The following mouse strains were used in this study: C57BL/6J, C57BL/6-Tg(UBC-GFP)30Scha/J, B6.SJL-PtprcaPepcb/BoyJ, B6.129P2-Apoetm1Unc/J, Nestin-GFP, LeptinRcre-R26-YFP and -R26-Tdtomato, OCN-GFTopaz, CD45.1STEM, and B6.Cg-Tg(Prrx1-cre/ERT2,-EGFP)1Smkm/J crossed with B6.129P2-Leprtm1Rck/J. Seven- to eight-week-old mice of both genders were used for experiments.

Wild animals

This study did not involve wild animals.

Field-collected samples

This study did not involve field-collected samples.

Ethics oversight

All experiments were approved by the Subcommittee on Animal Research Care at Massachusetts General Hospital. All efforts were made to minimize suffering.

Note that full information on the approval of the study protocol must also be provided in the manuscript.

Human research participants

Policy information about [studies involving human research participants](#)

Population characteristics

The population characteristics for The Canakinumab Anti-Inflammatory Thrombosis Outcomes Study (CANTOS) are described in Ridker et al. (Ridker PM, Everett BM, Thuren T, MacFadyen JG, Chang WH, Ballantyne C, Fonseca F, Nicolau J, Koenig W, Anker SD, Kastelein JJP, Cornel JH, Pais P, Pella D, Genest J, Cifkova R, Lorenzatti A, Forster T, Kobalava Z, Vida-Simiti L, Flather M, Shimokawa H, Ogawa H, Dellborg M, Rossi PRF, Troquay RPT, Libby P, Glynn RJ; CANTOS Trial Group. Antiinflammatory Therapy with Canakinumab for Atherosclerotic Disease. *N Engl J Med.* 2017; 377(12): 1119-1131). Multivariate regression analyses were used to address for effects after adjustment for age, gender, body mass index, education level, history of heart failure and hemoglobin A1c.

From the Athero-Express registry, 913 participants (mean age of 68.9 years, 73.1% males) were included in this study. Patient characteristics of the Athero-Express cohort are in detail listed in Supplementary Table 3.

Recruitment

CANTOS:

Patient recruitment was performed at participating centers in 39 countries. Patients were eligible for enrollment if they had a history of myocardial infarction and a blood level of high-sensitivity C-reactive protein of 2 mg or more per liter despite the use of aggressive secondary prevention strategies. Additional details on patient recruitment are listed in Ridker et al. (Ridker PM, Everett BM, Thuren T, MacFadyen JG, Chang WH, Ballantyne C, Fonseca F, Nicolau J, Koenig W, Anker SD, Kastelein JJP, Cornel JH, Pais P, Pella D, Genest J, Cifkova R, Lorenzatti A, Forster T, Kobalava Z, Vida-Simiti L, Flather M, Shimokawa H, Ogawa H, Dellborg M, Rossi PRF, Troquay RPT, Libby P, Glynn RJ; CANTOS Trial Group. Antiinflammatory Therapy with Canakinumab for Atherosclerotic Disease. *N Engl J Med.* 2017; 377(12): 1119-1131).

Athero-Express:

Patient recruitment was performed at University Medical Center Utrecht (UMCU, the Netherlands). Patients undergoing carotid endarterectomy or femoral vascular procedures were eligible for enrollment. Additional details on patient recruitment are listed in Verhoeven et al. (Verhoeven BA, Velema E, Schoneveld AH, de Vries JP, de Bruin P, Seldenrijk CA, de Kleijn DP, Busser E, van der Graaf Y, Moll F, Pasterkamp G. Athero-express: differential atherosclerotic plaque expression of mRNA and protein in relation to cardiovascular events and patient characteristics. Rationale and design. *Eur J Epidemiol.* 2004; 19(12): 1127-33) and Hellings et al. (Hellings WE, Moll FL, de Kleijn DP, Pasterkamp G. 10-years experience with the Athero-Express study. *Cardiovasc Diagn Ther.* 2012; 2(1): 63-73).

Ethics oversight

CANTOS: The study protocol was approved at participating centers by the responsible institutional review board or ethics committee, as applicable in the 39 countries involved. An independent data and safety monitoring committee oversaw the trial. Athero-Express: The study protocol was approved by the medical ethics committee of the UMCU.

Note that full information on the approval of the study protocol must also be provided in the manuscript.

Flow Cytometry

Plots

Confirm that:

- The axis labels state the marker and fluorochrome used (e.g. CD4-FITC).
- The axis scales are clearly visible. Include numbers along axes only for bottom left plot of group (a 'group' is an analysis of identical markers).
- All plots are contour plots with outliers or pseudocolor plots.
- A numerical value for number of cells or percentage (with statistics) is provided.

Methodology

Sample preparation

Sample preparation is described in detail in the Methods section.

Instrument

LSRII (for flow cytometry) and FACSaria II (for cell sorting), both BD Biosciences.

Software

FACSDiva v8.0.3 (for acquisition) and FlowJo v10.3.0 (for analysis).

Cell population abundance

The purity of sorted cells was >95%.

Gating strategy

The gating strategy is described in the Methods section and gating strategies are provided either in main figures or extended data figures. All samples were pre-gated on viable and single cells (FSC-A vs FSC-W, and SSC-A vs SSC-W).

Tick this box to confirm that a figure exemplifying the gating strategy is provided in the Supplementary Information.